Diffusion in an Absorbing Porous Medium: from Microscopic Geometry to Macroscopic Transport

by

David C. Forney III

B.S. Mechanical Engineering, University of Delaware (2003)

Submitted to the Department of Mechanical Engineering
in partial fulfillment of the requirements for the degree of

Master of Science in Mechanical Engineering

at the

MASSACHUSETTS INSTITUTE OF TECHNOLOGY

February 2007

Author .....
Department of Mechanical Engineering
January 31 , 2007

Certified by .....
Daniel H. Rothman
Professor
Thesis Supervisor

Certified by .....
Anette Hosoi
Professor
Department Advisor

Accepted by .....
Lallit Anand
Chairman, Department Committee on Graduate Students

Diffusion in an Absorbing Porous Medium: from Microscopic Geometry to Macroscopic Transport

by

David C. Forney III

Submitted to the Department of Mechanical Engineering
on January 31 , 2007, in partial fulfillment of the
requirements for the degree of
Master of Science in Mechanical Engineering

Abstract

Two physical models of diffusion in absorbing porous media are proposed on two length scales. One models diffusion in the pore space of a random medium with absorbing interfaces while the other is a reaction diffusion model where particles are absorbed in the bulk. Typical particle travelling distances and a bulk absorption coefficient are described in terms of general geometrical characteristics of a random medium and the analytical relations are found to compare well with numerical experiments. For the case of geometries consisting of randomly placed cubes, absorption in the bulk scales with the solid fraction to the two-thirds power. The statistical distribution of reaction rates in these models is found to be inversely related to the reaction rate. A quasi-static Monte-Carlo model is also investigated. The more complex problem of microbial extracellular enzyme distributions in marine sediment was an inspiration for this work.

Thesis Supervisor: Daniel H. Rothman
Title: Professor

Acknowledgments

Special thanks to Dan for leading me along this rewarding endeavor.

I must acknowledge Alex Lobkovsky who provided great input from discussions regarding this problem.

Much gratitude towards Svea for being a superb role model in life and work. She is a true hero.

Contents

List of Figures

Chapter 1

Introduction

Reaction-Diffusion occurs in many engineering and natural processes. The aim of this thesis is to understand aspects of diffusion when reactions occur at interfaces within a random porous medium. One-species systems are investigated and we consider only diffusion limited reactions. We only consider steady systems where concentration sources are distributed throughout the porous medium. The main goal is ascertaining the flux at solid fluid interfaces of the porous media and the geometric properties that govern it.

1.1 Overview

Systems of this type are investigated at two scales, "microscopic" and "macroscopic". On the microscopic scale the system is modeled by the steady diffusion PDE in the pore space and boundary conditions with zero concentration on the porous interfaces. This is called the microscopic model.

$$0 = \nabla^2 C \qquad \text{in pore space} \tag{1.1}$$

$$-D\nabla C = j_a \qquad \text{on source boundary} \tag{1.2}$$

$$C = 0 \qquad \text{on interface boundary} \tag{1.3}$$

j_a is the source flux of concentration. This model is then analyzed numerically by solving (1.1)- (1.3) with ensembles of random boundary geometries. A 64x64x64 with grid with periodic boundaries was used for numerical simulations. A source

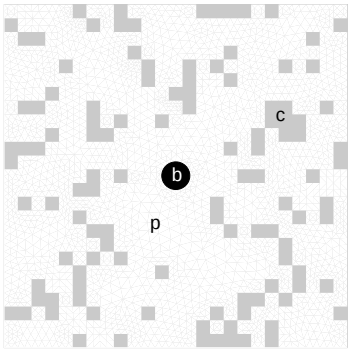

Figure 1-1: Geometry of 2-D microscopic model. b is the source, the pore space, p, is white. Random solid particles, c, are gray.

was placed at the center of the grid and the remaining domain inside the grid was filled with randomly spaced particles. A finite difference method was used to solve (1.1)- (1.3).

Reactions in the microscopic model were modeled as purely absorbing by setting the concentration to zero along the walls at the porous interfaces. This is a special case of the more robust radiative boundary condition [32] $D\nabla C = \alpha C$ where α is a constant absorption rate over the specific surface area. It was first introduced by Collins and Kimball for dilute spheres [32], [35]. Varying α/D from zero to infinity changes the system from being reaction-controlled to diffusion-controlled (diffusion-limited). Physically, low concentrations can arise at an interface if there is a high equilibrium ratio of substrate-sorbed to dissolved chemical species, or if the chemical species is eliminated very rapidly at the interface (diffusion limitation). This is described further in section 2.1. The radiative boundary condition provides a possible way to tackle the adsorption problem when there is a lower equilibrium ratio or lower saturation levels.

The macroscopic model on the other hand does not include pore geometry. It models the system as a continuum "mud" where the concentration adsorption on the walls of the porous interfaces is a volume averaged process occurring throughout the continuum. Specifically, the concentration is modeled by the steady reaction diffusion equation.

$$0 = \bar{D}\nabla^2 c - \kappa c \qquad \text{in continuum} \tag{1.4}$$

$$j_a = -\bar{D}\nabla c \qquad \text{on source boundaries} \tag{1.5}$$

Note that C in equations (1.1)-(1.3) represents a concentration in pore space while c represents a macroscopic concentration in the mud. For the same reason, $\bar{D}$ is an effective diffusion coefficient.

Analysis for the "macroscopic" model is done analytically for a spherical volume in the neighborhood of a source.

1.2 Previous Work

There has been much prior work on systems closely related to the microscopic and macroscopic models described in section 1.1. It is more broadly known as the problem of diffusion to static traps. Although the roots of this problem can be traced to Smoluchowsky and the more general studies of diffusion controlled reactions, Bixon and Zwanzig [3] were the first to use the term static traps, however Felderhof and Deutch [10] tackled almost the same problem years earlier. General problem of static traps is to find effective macroscopic properties of the microscopic system described earlier. Absorbers are large and stationary with respect to the diffusing particles around them and diffusion limited reactions occur on the surfaces of the traps. Properties of interest are survival time of a particle, relaxation times, effective reaction rates, and diffusion coefficients. The general way this problem was originally solved was to re-write the boundary conditions of the microscopic equations to create a modified microscopic model where the boundary conditions are incorporated into a reaction term. This was first done by Fixman [36] for diffusion controlled reactions. There are many ways to do this but all of them are complex and come from the solutions to other known problems in physics. Then quantities of interest are averaged in order to get the bulk property desired. Felderhof and Deutch were the first to propose locally averaging the modified microscopic equation to get the macroscopic relation (1.4), where κ is a function of geometry only. However, the validity of that local microscopic averaging is questionable [30]. Effective medium properties were further studied in this way by many [7],[19],[11],[6] and more.

It wasn't until later that that the static trap problem was properly addressed

for higher solid fractions of traps and branched into a problem that can be thought of as diffusion through a heterogeneous medium with static traps. Before, most analysis done was for traps not near touching each other with solid fractions of around 0.1 or less. Note that getting to that solid fraction was a huge improvement over the Smoluchowsky model [32] [35] which is only valid for extremely low absorber concentrations $\ll 0.1$. When higher solid fractions are considered, the problem can be more thought of as diffusion through a heterogeneous medium consisting of static traps. Doi [7], Muthukumar [19] and Fixman [11] tastefully worked on the early stages of this problem, but later Richards and Torquato made much more headway in this topic. Richards tackled the high solid fraction problem via analysis and computations of random walks while Torquato utilized his pioneering work regarding the mechanics of heterogeneous material in conjunction with the methods of Doi and Muthukumar. A comparison of their results with our cubic system is presented in section 4.3.3.

1.3 Motivations

The problem of carbon burial in the ocean is an important aspect of the carbon cycle and is not fully understood. Micro-organisms are known to be key players in the degradation of organic matter in the ocean [1]. Microbial decay on the ocean floor is the final stage of respiration before organic carbon is buried.

It has been found that the amount of particulate organic carbon (POC) is strongly correlated with the surface area of minerals(clay) in the sediment [15],[14]. This leads to the assumption in our models that POC exists as coating on surfaces of clay. Our work was also inspired by the discussion of extracellular enzyme foraging by Vetter [34]. To forage, extracellular enzymes are released from microbes in the sediment compound. The enzymes diffuse through pore spaces and catalyze the hydrolysis of POC, resulting in the release of dissolved organic carbon(DOC).

This process is modeled via steady reaction diffusion with boundary conditions mentioned in section 1.1. This process and idealized system geometry is shown in figure 1-2. Our model assumes that the spacing of bacteria (spacing of sources) is much greater than the typical pore size of the medium. The model works best when the characteristic foraging distance of an active extracellular enzyme (diffusing particle), β^{-1}, is much less than the bacterial spacing $\sim r_b$. This is discussed further in section 3.2.

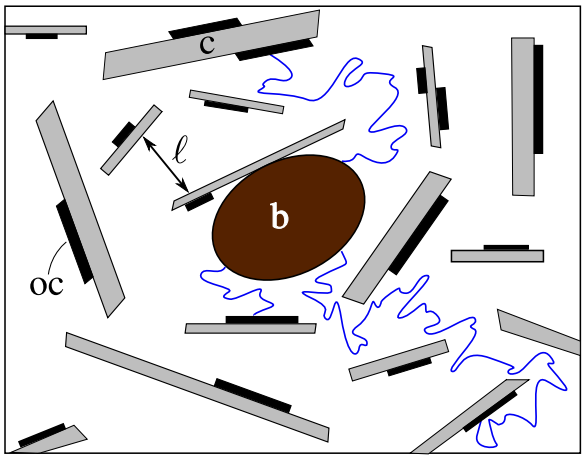

Figure 1-2: Idealized sediment geometry and enzyme release process

Although the models presented in this thesis were inspired by the detrital degradation problem in marine sediment, these models *are not* the physical models mentioned in our publication [25]. Although the two types of models are related, the model in the *Science* publication assumes a characteristic enzyme lifetime while these thesis models assumes contact with a wall ultimately ends the activity of an enzyme; it is either irreversibly adsorbed or denatures while adsorbed.

There are numerous assumptions with the thesis reaction diffusion models of the enzyme foraging process. These models assumes enzyme elimination at walls, but it is difficult to gauge how unreasonable this assumption is . Typical sizes of extracellular enzymes are in the range of 10-1000 KDa [34]. Large polymers often adsorb irreversibly to clay minerals [20], and new techniques for measuring adsorption show that adsorption of polysaccharides in minerals can be high depending on polysaccharide type and mineral type and density [29]. As the equilibrium fraction of adsorbed to dissolved enzymes increases, our assumption is more reasonable. If enzymes are significantly less likely to denature while adsorbed rather than dissolved, then this assumption seems less likely. If enzymes are more likely to denature during adsorption then the strength of this assumption improves. Secondly, why should steady flux from the source be assumed if over time, fewer and fewer OC remains in the environment as food for the microbe? A peculiarity of this specific diffusion model is that the concentration of enzymes remains in a steady state spatially even though the OC in the local environment disappears. Therefore, it is easily argued that this reaction diffusion system does not model the microbial decay of organic carbon in marine sediment. The model has other shortcomings as well but nevertheless, this

physical problem was a source of inspiration for the mathematical model discussed here.

In order to address some of the supposed conflicts with reality associated with the simple diffusion model, a reaction-diffusion Monte-Carlo model was also analyzed. In the Monte-Carlo simulations, POC was removed from the system over time. Under comparison with published experimental data, the results of this model were not as promising as the fully steady model. This Monte-Carlo model is discussed in chapter 5.

In addition to the problem of enzymatic decomposition, there are other reaction - diffusion problems in porous media. These range from physical and biological problems to problems in engineering.

- Enzymatic infection of soft tissue
- Oxygen absorption in lungs
- Heterogeneous catalysis, catalytic converter
- Batteries
- PEM fuel cells
- Hydrogen storage in metals

1.4 Objectives

The main goal of this work is to connect two length scales of diffusion in an absorbing random medium. Specific tasks are to address fundamental questions about the system such as determining how the concentration decays from the source as well as how the flux to interfaces is distributed. Another task is to look at the effect of geometric parameters such as porosity and surface area on the system behavior. The macroscopic reaction diffusion PDE must be shown to be an accurate model of the microscopic diffusion model with random absorbing boundaries. Given that the microscopic and macroscopic PDEs model the same system, the scales can be connected by explaining how microscopic geometry affects macroscopic transport and absorption.

Chapter 2

Microscopic Model

2.1 Diffusion and Absorbing Boundaries

The backbone of this problem is the molecule. In many biological environments, only trace concentrations of a chemical species exist. The continuum model presented in this chapter describes systems with large concentrations(Kn $<<$ 1), but also describes time-averaged concentrations in diluted systems. Although it is useful to think about this problem on the molecular level, all analysis will be done on the continuum level. The behavior of a concentration of a species in a in a solution can be described by the diffusion equation.

$$\frac{\partial C}{\partial t} = \nabla^2 C \tag{2.1}$$

Assuming that the steady microbe source and the geometry surrounding it moves on a timescale slower than diffusion, the time derivative can be neglected in (2.1).

The porous geometry of ocean floor sediment is complex. To keep things simple, the model's geometry consisted of placing cubes down on a cubic grid at random. Porosity is the only parameter in this simple cubic model.

Possible physical scenarios with absorbing boundaries

The boundary condition on the surfaces of the cubes is $C = 0$, implying that there is no communication between the surface and the surrounding pore space, hence the term "absorbing boundaries". It is shown here that absorbing boundary conditions are appropriate if contact with the surface results in the particle either becoming trapped or eliminated.

Transport involving surfaces is typically modeled with rate constants[4] which describe the exchange between dissolved concentrations and concentrations which are adsorbed to the substrate surface. The dissolved concentration in a pore-space volume element with length δx in the x direction may be described by

$$\frac{dC}{dt} = D\nabla^2_{2D} - \frac{j_+}{\delta x} + \frac{j_-}{\delta x} \tag{2.2}$$

where ∇^2_{2D}, is the 2-D Laplacian operating in the YZ plane. For a volume element surrounded by pore space, the fluxes j_+, j_-, through the surfaces at $x + \delta x/2$ and $x - \delta x/2$, are simply fluxes due to diffusive transport and the r.h.s. of (2.2) reduces to $D\nabla^2 C$. However, if the volume element borders a solid surface, transport to and from surface is described by rate constants resulting in the relation,

$$\frac{dC(\mathbf{x})}{dt} = D\nabla^2_{2D} - k_a C(\mathbf{x}) + k_d \frac{C_s}{\delta x} + D\nabla C(\mathbf{x} + \delta \mathbf{x}/2). \tag{2.3}$$

with k_a being the rate constant for adsorption to the surface and k_d being the rate constants for desorption from the surface both having units inverse time. C_s is the concentration per unit surface area and the 4^{th} term represents the diffusive flux j_+. If adsorption is diffusion limited, the transport to the boundary surface is solely due to diffusion so $k_a = \frac{D}{\delta x^2}$. Therefore diffusion limitation results in

$$\frac{dC}{dt} = D\nabla^2_{2D} - \frac{D}{\delta x^2} C + \frac{k_d}{\delta x} C_s + D\nabla C(\mathbf{x} + \delta \mathbf{x}/2). \tag{2.4}$$

Discretizing equation (2.4) shows that either $k_d = 0$ or $C_s = 0$ is sufficient for absorbing boundary conditions to be present. Physically, $k_d = 0$ means what contacts the boundary is not released, and $C_s = 0$ means contact with the boundary results in rapid elimination. To see this consider the equilibrium distribution of surface molecules governed by the equation

$$\frac{dC_s}{dt} = k_a C \delta x - k_d C_s - \alpha C_s \tag{2.5}$$

where α is a death rate of molecules on the surface. Steady state results when

$$C_s = \frac{k_a \delta x}{k_d + \alpha} C \tag{2.6}$$

Since k_a is controlled by diffusion, C_s approaches zero when α approaches ∞. Physically, large α might occur if enzymes are more prone to denaturing during

hydrolysis, or surface molecules are more prone to denaturing the enzyme.

To be more precise, $\alpha/k_d \gg 1$ indicates that most *adsorbed* particles are destroyed rather than released. This is also sufficient to indicate the significance of absorbtion relative to our model. It is important to realize that the equillibrium ratio of sorbed to pore dissolved particles is not alone sufficient to determine the degree to which a medium is absorbing for our purposes. In this thesis absorbing is used in the *first passage* sense. In other words, if the particle is more likely to be released rather than eliminated while sorbed, then the medium is less absorbing. If it is more likely to be eliminated at contact with the first boundary, it is more absorbing. There might be orders of magnitude more particles sorbed than in the pore space, but if they are all released before they are eliminated, then the absorbing model discussed here does not apply. In order to estimate real values of α/k_d, note that $\alpha \sim 10^{-3}$s nominally in sea water and $C_s/C \sim 10^{-3}$cm [34]. If δx in (2.6) is taken to be roughly a pore size l (questionable assumption), then

$$\frac{C_s}{C} = \frac{k_a}{k_d + \alpha} l \tag{2.7}$$

$$\frac{C_s}{C}\frac{s}{\phi} = \frac{k_a}{k_d + \alpha}\frac{sl}{\phi} \tag{2.8}$$

$$\frac{C_s}{C} \sim \frac{k_a}{k_d + \alpha} \tag{2.9}$$

Plugging in values for the equillibrium ratio and known specific surface area $s \sim 10^5$cm and $sl \approx 1$ gives

$$\frac{k_a}{k_d + \alpha} \sim 10^2. \tag{2.10}$$

An estimate of the order of magnitude of k_a or k_d is needed. The dynamics of adsorption on various minerals of large molecular weight polymers have recently been studied by Steen and Arnosti [29]. Ranges of adsorption timescales were found. Noting that the labeling technique was stable, a more simple model can be used to find k_a for large MW polymers. Again utilizing a linear adsorption-desorption model,

$$\dot{C}^* = -C^* k_a + C_s^* k_d \tag{2.11}$$

$$\dot{C}_s^* = C^* k_a - C_s^* k_d \tag{2.12}$$

Where C^* and C_s^* are total amounts of pore dissolved and sorbed polymers. Since

$C^* + C_s^* = C_{tot}^*$, the dynamics have a first order rate constant of $k_a + k_d$. Since $k_a > k_d$, the dynamics of the system can be attributed to k_a. Rates inferred from [29] varied from $10^{-4} < k_a[1/s] < 10^{-2}$ for the various polymers and substrates tested. Of course various enzymes adsorb to various substrates, some more reversible than others, but using k_a as an estimate for similar molecular weight enzymes, results in a conservative estimate of k_d using the equillibrium ratio (2.10) $10^{-6} < k_d[1/s] < 10^{-4}$. Therefore using a simple linear model of adsorption with these values of sorption coefficients and death rates, this medium is approximately first passage absorbing. However since the range of α spans over 6 orders of magnitude resulting in α/k_d spanning 10^{-1} to 10^6 [34] and sorption varies widely depending on enzyme and mineral, no definite conclusions can be made.

2.2 Numerical Solution of Microscopic Problem

Because solving Laplace's equation on a random domain is difficult analytically, numerical simulations are used to analyze this problem. A source of constant strength is placed at the center and the outer boundaries of the numerical domain are set as periodic. Therefore the numerical simulations are actually models of a porous domain with regular array of sources separated by a distance the length of the simulation domain.

2.2.1 Two Dimensional Problem

The problem was first attacked in two dimensions. As in the 3-D problem, the porous geometry was created by squares placed randomly in a two dimensional rectangular domain, with periodic boundaries defining the outer edges of the domain. The finite-element method in Matlab's PDE toolbox was used. Although very robust, the stock PDE toolbox was not able to handle repeating boundaries, so the toolbox was modified to include repeating boundaries. Because the toolbox was easy to use and simulations were created quickly, there was a tradeoff in performance. A domain of length 100 grain sizes was the largest simulated.

Results

The information most relevant to the problem of biodegradation is the flux of enzymes to the particulate carbon. Since reactions are assumed to be diffusion limited and

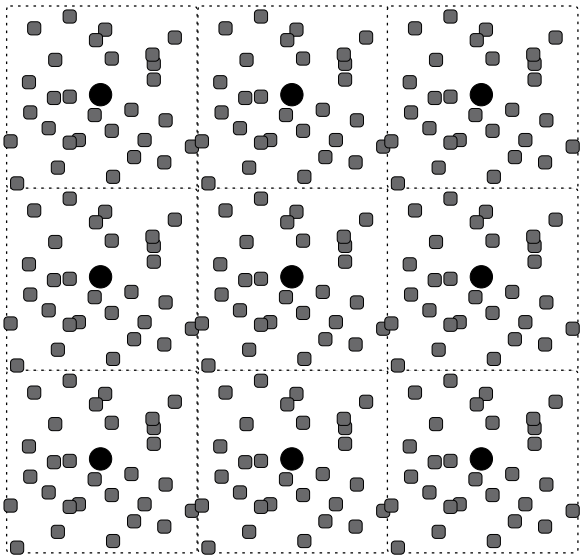

Figure 2-1: Geometry of microscopic model with periodic boundary conditions. Dashed lines indicate the periodic boundaries on the outer boundary of the simulation. Black circles are sources, and gray blocks are grains.

carbon is assumed to be completely covering the walls of the porous surface, the flux to the wall is a very important quantity. Flux to the walls is defined as

$$j_w(\mathbf{x}) \quad = \quad -D\nabla C(\mathbf{x}) \cdot \mathbf{n}, \ \mathbf{x} \in \Gamma \tag{2.13}$$

with Γ being the set of points on the porous boundary and $\mathbf{n}$ being the vector normal to the boundary. Figures 2-2 and 2-3 show a spacial distribution of flux to the walls.

The porosity ϕ, is defined as the fraction of volume occupied by pore space. The figures show rapid decay of flux from the source for $\phi = 60\%$. The rapid decay is a consequence of the absorptive boundary conditions. Decreasing porosity reduces the likelihood of a molecule diffusing far from the source. Note that in figure 2-2, there are sections untouched by the source due to enclosures by the solid particles. Also note that there is a region of low flux to the left of the source. This is also due to enclosures, but the periodic boundary condition allows access to this region from the source to the left of it. Regions in the domain become more isolated as the solid fraction, σ defined as $\sigma = 1 - \phi$, approaches the percolation threshold for 2-D square lattice site percolation, $\sigma = p_c = .59$. [28]. Porosities lower than p_c cutoff the source from its extended environment. This may or may not be important as the source does not effect surfaces more than a few grain sizes away from it. In three dimensions, cutoff happens not when solid percolation occurs, but when pore space percolation

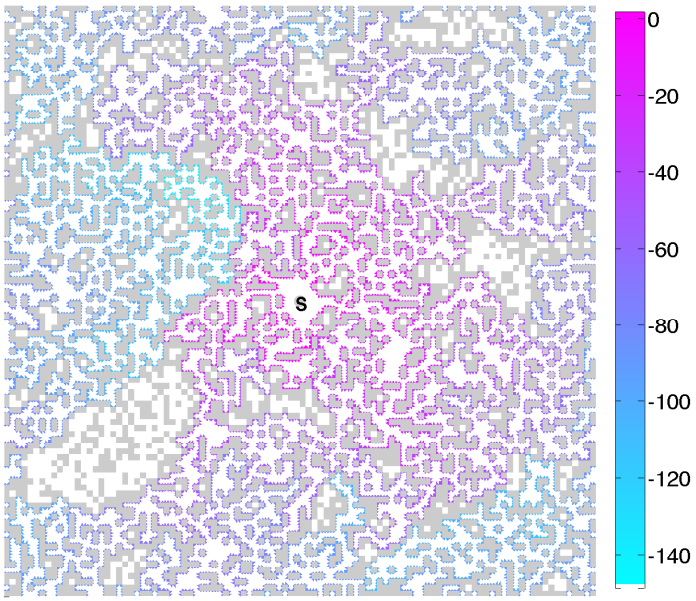

Figure 2-2: Spacial distribution of flux to the walls. The source is donated by the letter S. The pore space adjacent to each wall is highlighted with a color indicating the flux to that wall. Colorbar is $\log_{10}(j_w)$. The porosity, $\phi = 60\%$.

does not occur. This happens when the porosity equals the percolation threshold for 3-D simple cubic site percolation, $\phi = p_c = .31$. [28]. Intuitively, the critical porosity is lower in 3-D because it is much harder to enclose volumes than areas.

By binning all of the wall fluxes in the domain, this two dimensional information is reduced to a histogram called the harmonic measure. The fluxes are binned logarithmically and is shown in figure 2-4.

Important qualitative concepts to take away from figures 2-2- 2-4 is that very few surfaces see high flux and few surfaces see low flux. The trend in the high flux portion of figure 2-4 is explained by geometry. The number of surfaces increases with distance, but the flux decays with distance. The tail of the histogram at low flux is actually due to the randomness of the model. Although the tail does have to do with measuring the harmonic measure in a finite volume, the tail is not a typical finite size effect. One would expect the number of low flux surfaces to fall off as the wall flux approaches the minimum in the domain, but that is not so obvious when log binning is used. This is discussed further in the next section.

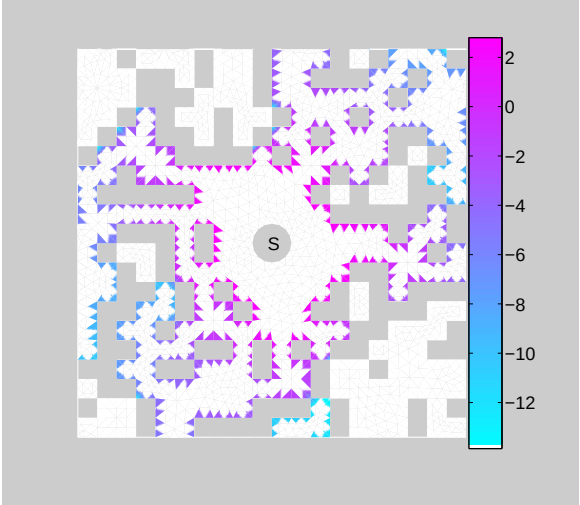

Figure 2-3: Zoomed in close to the source. Again the colorbar is $\log_{10}(j_w)$ and source is labeled S. $\phi = 60\%$

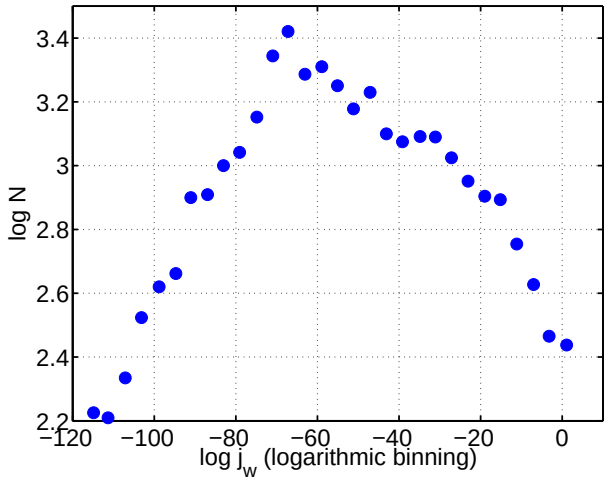

Figure 2-4: Histogram of fluxes to walls, j_w, binned logarithmically. N is the number of surfaces with corresponding j_w.

2.2.2 Three Dimensional Problem

Equations (1.1)- (1.3) were solved in three dimensions using a finite difference scheme on a 64x64x64 grid. The grid spacing, h is one half of a grain length[1] so each grain has edges comprised of three nodes. Nodes are located on the exact surface of the grain has volume 2^3. Surface nodes have have concentrations set to zero corresponding with the $C = 0$ boundary condition. Again periodic boundaries are used at the domain edges and the source is located at the center of the grid. The relaxation method used

[1] A discussion of the accuracy of the results for such a coarse discretization is in section B.1

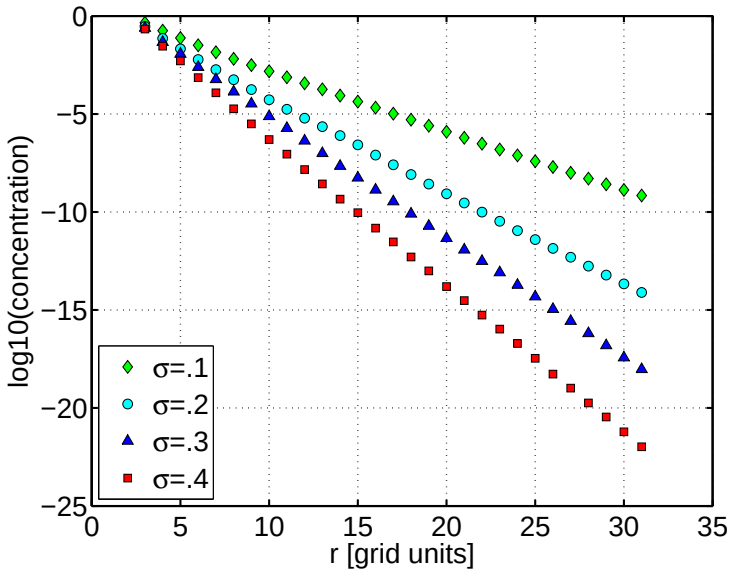

Figure 2-5: log10(Radially averaged concentration) vs. Distance from the source.

to solve this problem was Gauss-Seidel[2]

Results

Important results from this model are the concentration decay with distance from the source and the harmonic measure of flux to walls. In order to draw accurate conclusions from simulations with stochastic boundary geometries, an ensemble of numerical experiments was performed. Ten experiments were performed for each porosity tested.

To measure how the flux decays with distance from the source for a given porosity, the concentration was radially averaged in each experiment, then the ensemble of concentration profiles was averaged resulting in figure 2-5. Note that the concentration decay seems to be exponential. The solid fraction has a strong effect on the decay of concentration. Increasing the σ by .1 changes the concentration at a given distance by a few orders of magnitudes.

A histogram is again used to describe the flux to the walls, j_w. Only walls located at a distance $r \leq \frac{L}{2}$ were counted, where L is the length of the simulation domain. The fluxes were binned logarithmically and the frequency normalized to 1 for each experiment resulting in the harmonic measure, H_l. Then the ensemble averages of $\log 10(j_w)$ and $\log 10(H_l)$ were computed resulting in figure 2-6. $H_l(\log(j_w))$ is labeled

[2]Gauss-Seidel was found to converge very quickly for problems of this type, see appendix B.

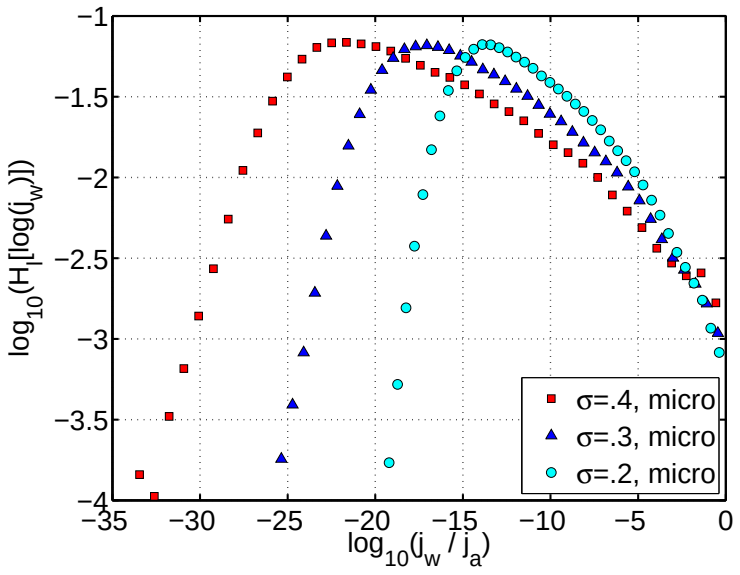

Figure 2-6: Probability distribution of flux to walls, $\log_{10}(j_w/j_a)$ for various solid fractions. Fluxes are binned logarithmically. j_a is the source flux.

to emphasize that H_l is the distribution of the *log* of the flux. A turnover is seen similar to the one in the 2-D simulation. It is important to note the maxima in the histogram, figure 2-6, corresponds to the minimum seen in figure 2-5. This is not to say that the flux to the walls is the concentration at that location, but that the flux is scales with concentration (since $j_a = 1$ in this simulation, j_w/j_a is of similar magnitude as concentration.) Because only walls located distance $r \leq \frac{L}{2}$ were binned, this is a clue explaining why the tail in the figure must be due solely to random low flux surfaces in the domain.

Another, perhaps more intuitive take on this distribution is to bin the fluxes linearly as shown in figure 2-7. The log-binned histogram is converted to a linear binned histogram by the operation,

$$\frac{H(\log(j_w))}{ln(10)j_w} = H(j_w), \tag{2.14}$$

where H is the linearly binned probability distribution. This conversion was necessary since there is not nearly enough data to linearly bin the data on the log scale required.

Note that this figure is more intuitive than the last one as the number of walls always increases as flux decreases. What appears to be counter-intuitive is the pdf itself. It does not seem to integrate to one like the log-binned plot. This is because now

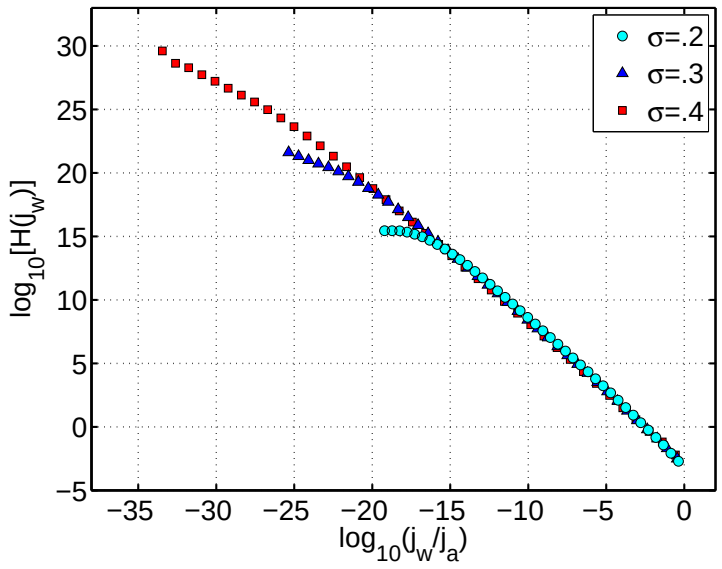

Figure 2-7: Probability distribution of flux to walls, $\log_{10}(j_w/j_a)$ for various solid fractions. Linear binning.

the width of each bin is orders of magnitude smaller. The portion above $\log_{10}(H) = 0$ accounts for only an extremely small fraction of the flux domain, so it does indeed integrate to one. Note that the location of the non-linearity in figure 2-7 corresponds to the location of the maxima in figure 2-6.

Chapter 3

Macroscopic Model

3.1 Reaction Diffusion in the Bulk

The microscopic model can also be reformulated on the macroscopic scale. Consider a homogeneous, isotropic mud where the microstructure of the clay is too small to be noticed. Diffusion and adsorption still take place, but now are considered to be bulk processes. Again, sources are considered to be distributed throughout the mud. The macroscopic concentration is $c = \langle C \rangle \phi$, where $\langle C \rangle$, is the average concentration in the pore space. This system is modeled by the reaction-diffusion equation,

$$\partial_t c = \bar{D} \nabla c - \kappa c, \tag{3.1a}$$

where $\bar{D}$ is an effective diffusion coefficient for the porous medium and κc is a bulk absorption rate per unit volume since on the macroscopic scale particles are being consumed in the continuum. Utilizing a macroscopic equation where κ and $\bar{D}$ are a function of geometry only was first done by Felderhof and Deutch [10].

It was later shown by Tokuyama and Cukier [30] that one cannot re-write the microscopic model (2.1) with Dirichlet boundary condition (1.3) as the locally averaged macroscopic form (3.1a) when the characteristic foraging distance, β, of a particle is on the order of absorber size l_g. This arises because fluctuations on the local scale do not average out at all larger scales. Unfortunately, those length scales are of similar order for most porous media with $\sigma > 0.1$. Tokuyama and Cukier's result that fluctuations exist on all length scales can be seen by looking at figures 2-2, 2-3, and D-1. In these figures one can observe that radially averaging only picks out the highest flux at that radius because fluxes vary over many orders of magnitude. Therefore

radially averaging will not yield an effective absorption per unit volume, because that concentration represents only the highest concentration at a point in that volume. Compare figure D-1 to the line labeled $\sigma = 0.3$ in 2-5. Since the concentration at the source is ~ 1 in fig. 2-5 and we are normalizing the flux in fig. D-1, the concentration is roughly the same as the flux and we can compare the two quantities. At $r = 30$, the concentration is $\sim 10^{-17}$ in figure 2-5. At $r = 30$, the flux varies from $\sim 10^{-17}$ to $\sim 10^{-23}$. Because of the averaging, only 10^{-17} is counted and this is considered the average for $r = 30$, when in reality it is fluctuating at all scales over several orders of magnitudes as seen in figs 2-2, 2-3, and D-1. This is discussed as well in Appendix D. The implications of this are curious and hardly discussed in the literature. What this means for us is that β is really estimating is how the "safest paths" scale with microstructure. What we have found below is that radially averaging produces a well behaved concentration from the source, so these paths must be changing in accordance with our model. But if we were to plot the actual macroscopic concentration in 3D, it would be fluctuating at all scales, look at fig. 2-2. Mapping the 3D concentration to 1D brings some order to the chaos of Tokuyama and Cukier's result. Since the averaging represents some sort of scaling of safest paths, it is not clear of the geometry of these paths and whether each maximum concentration is part of one long path or does the concentration jump among paths. The scaling regarding these paths and maximum concentrations are not understood. Given these comments, it is still questionable what exactly the actual absorption is in the bulk volume and what $\kappa c(r)$ represents.

Regardless of this finding, many continue to find effective medium properties and most [23], [6], [32] continue to use (3.1a). As shown later in this chapter, analysis of the macroscopic model seems to be sufficient to describe β for our discretized microscopic system even for $\beta \lesssim l_g$.

As in the microscopic model, the assumption of a steady source and boundaries which are changing very slowly allow neglection of the time derivative. Results from the micro model indicate that the concentration in a given of mud should should only be effected by the nearest source. This is inferred from the high sensitivity of concentration with distance from a source. In other words, each source has a sphere of influence of radius r_b, where $2r_b + \epsilon$ is the distance to the nearest neighboring source, $\epsilon \ll r_b$. We will shortly show what conditions are required for high distance sensitivity.

The problem can now be restated in spherical co-ordinates.

$$0 = \bar{D}\frac{1}{r^2}\frac{d}{dr}\left(r^2\frac{d(c(r))}{dr}\right) - \kappa c(r) \tag{3.2a}$$

$$c(a) = c_0 \tag{3.2b}$$

$$c(r_b) = c_b \tag{3.2c}$$

a is the radius of the source. Note c_b does not need to be coupled to the neighboring source since the neighboring source has negligible effect at $r = r_b$.

The solution to the steady state system (3.2) is [18]

$$c(r) = A\frac{e^{-\beta r}}{r} + B\frac{e^{\beta r}}{r} \tag{3.3}$$

$$A = \frac{c_b r_b e^{\beta a} + c_0 a e^{\beta r_b}}{e^{\beta(-r_b+a)} - e^{-\beta(r_b+a)}}, \qquad B = \frac{-c_b r_b e^{-\beta a} + c_0 a e^{-\beta r_b}}{e^{\beta(-r_b+a)} - e^{-\beta(r_b+a)}},$$

where $\beta = \sqrt{\frac{\kappa}{\bar{D}}}$. Note that $r_b \gg a$ for typical source spacing[1] and $c_0 \gg c_b$ for typical concentration decay, resulting in $A \gg B$. This means that the growing exponential does not play a role until $r \approx r_b$ but at that distance, $c \approx 0$ anyway. In other words, the growing exponential can be neglected. These assumptions result in

$$A = c_0 a e^{\beta a} \tag{3.4}$$

$$c(r) = \frac{c_0 a}{r}e^{-\beta(r-a)} \tag{3.5}$$

Profile. (3.5) is also the solution to equation (3.2) with outer boundary condition $c(\infty) = 0$.

As seen from radial profiles. (3.3)-(3.5), β plays a very important role. Physically, β^{-1} represents a characteristic distance traveled from the source before a molecule is captured. It is dependent on typical pore sizes in the microscopic geometry and sets the scale for many system characteristics.

3.2 Results of the Reaction Diffusion Model

It must be shown that the reaction diffusion model is an appropriate macroscopic representation of the microscopic system.

[1] $r_b \sim 10\mu m$ [26], $a \sim 0.5\mu m$ [34]

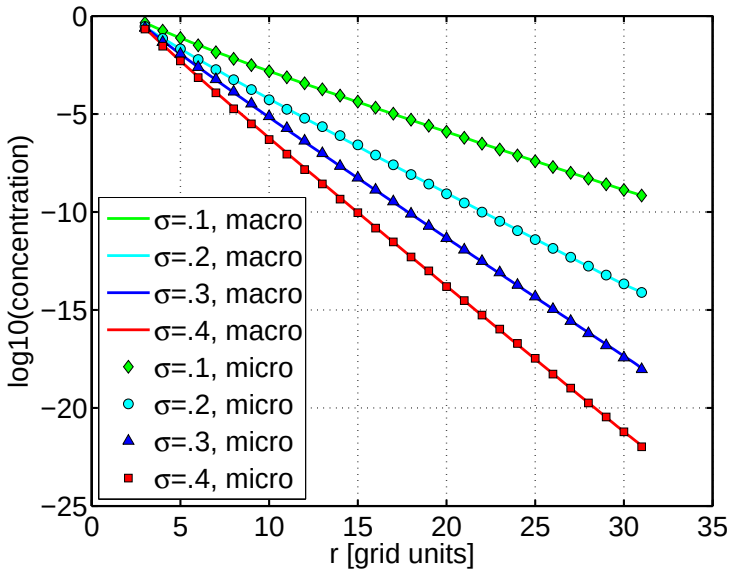

Figure 3-1: Concentration vs. r for various σ. Lines represent macroscopic solution with fitted boundary condition and β.

3.2.1 Concentration Profile of the Macroscopic Model.

The first thing to show is that solutions from the macroscopic reaction-diffusion model can indeed give the same volume-averaged results from the microscopic model. This is done graphically in figure 3-1.

For each value of σ the boundary conditions A,B were set equal to the radially averaged concentrations at $r = a, r_b$. Note the result is the same if B was set to zero. The macroscopic parameter β was determined by a best fit. As you can see, the macroscopic model does indeed seem to give the same results for $c(r)$ as the averaged microscopic data. Remember that $c(r)$ is not a pure exponential, but $c(r) \propto \frac{1}{r}e^{-\beta r}$. The $\frac{1}{r}$ influence is not seen in the plot because it changes too slowly as r departs from a and the exponential dominates from $r > a$. A key property of this model is exponential decay for $\beta r \gg 1$.

Insight from the solution, (3.4), tells us that an appropriate non-dimensionalization for $r - a$ should be β. In figure 3-2, the microscopically averaged distance from the source is non-dimensionalized by β and the concentration by $\frac{1}{c_0}$. All data sets collapse nicely onto one line.

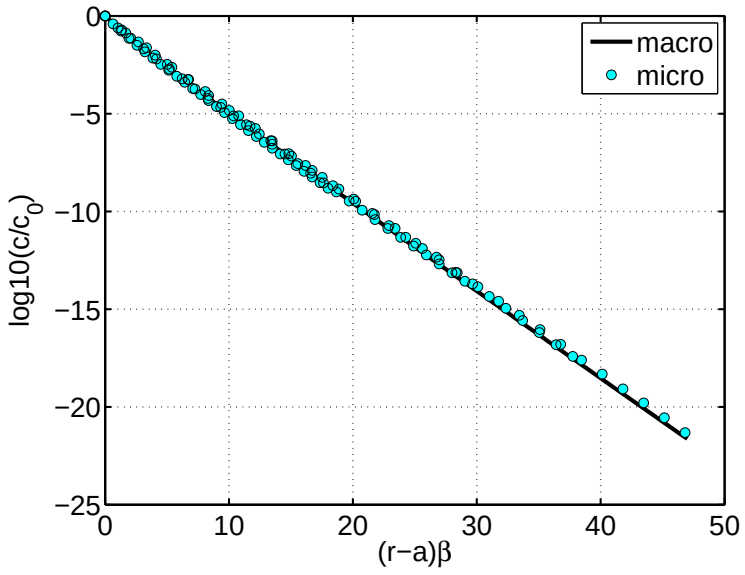

Figure 3-2: Normalized concentration vs. normalized distance from source surface, $r - a$

3.2.2 Flux Probability Density

In order to show further equivalence of the two models, the harmonic measure pdf, h, is calculated on the same spherical domain as the microscopic model. $h(j_w)$ is found analytically by considering $p(r)dr$, the probability of being located a distance $d \in [r, r + dr]$ from the source.

$$h(j_w) = p(r(j_w)) \left| \frac{dr}{dj_w} \right| \tag{3.6}$$

For $r_b \gg a$,

$$p(r) = \frac{3r^2}{r_b^3} \tag{3.7}$$

Knowing the bulk absorption rate $\kappa c(r)$ allows calculation of the flux $j_w(r)$.

$$j_w(r) = \frac{\kappa c(r)}{s} \tag{3.8}$$

$$j_w(r) = \bar{D} \frac{\beta^2 c(r)}{s} \tag{3.9}$$

where s $[\frac{1}{L}]$ is the specific surface area.

$$j_w(r) = \mathcal{A}e^{-\beta r}/r \qquad \text{where} \qquad \mathcal{A} = \frac{\bar{D}}{D}\frac{\beta^2 c_0 a e^{\beta a}}{s} \tag{3.10}$$

Because $j_w(r)$ is analytic, dr/dj_w is simply dj_w/dr^{-1}.

$$\frac{dj_w}{dr} = -j_w\left(\beta + \frac{1}{r}\right) \tag{3.11}$$

$$\frac{dr}{dj_w} = -j_w^{-1}\left(\beta + \frac{1}{r}\right)^{-1} \tag{3.12}$$

Again, j_w^{-1} dominates $\beta + \frac{1}{r}$ since $\beta r \gg 1$ so $\frac{dr}{dj_w} \sim j_w^{-1}\beta^{-1}$.

Analytical inversion of $j_w(r)$ requires the use of the Lambert-W function, $W(z)$, $z = We^W$.

$$r(j_w) = W(\mathcal{A}\beta/j_w)/\beta \tag{3.13}$$

therefore,

$$h(j_w) = |j_w^{-1}|\frac{3W(\mathcal{A}\beta/j_w)^2}{\beta^3 r_b^3(1 + 1/W(\mathcal{A}\beta/j_w))} \tag{3.14}$$

However, $h(j_w))$ can be analyzed without dealing with W. Defining $x = r/r_b$, Recognize that 98% of the volume of a sphere is located at a distance $x > .27$, thus $p(r)$ varies only by roughly one order of magnitude for most of the domain. This is negligible compared to the domination of j_w in $|dr/dj_w|$, and

$$h(j_w) \sim j_w^{-1}\beta^{-1} \tag{3.15}$$

$h(j_w)$ is plotted with the microscopic linearly binned harmonic measure $p(j_w)$ in figure 3-3. Note that the macroscopic model cannot capture the low flux stochasticity. This is of course because the low flux distribution is a random phenomena and cannot be captured with a macroscopic model. Figure D-1 in the appendix gives insight into this. The macroscopic ceases to give data for $j_w < j_w(r_b)$.

A prediction of the log-binned histogram can be converted from $h(j_w)$ with con-

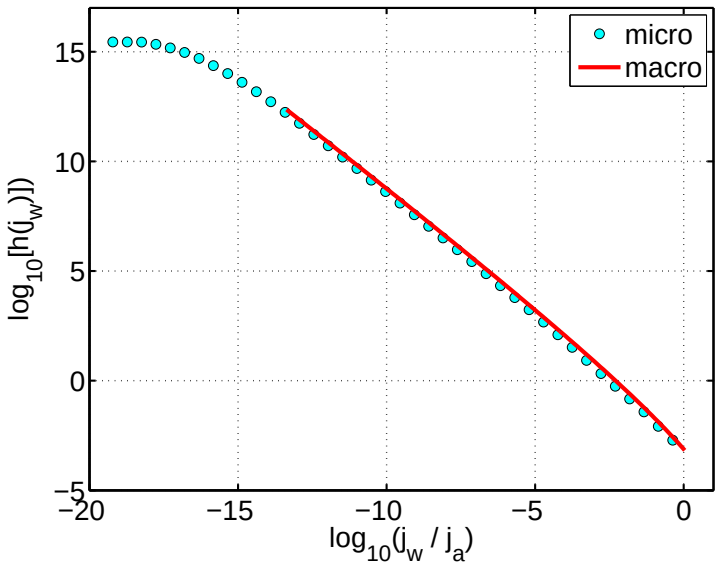

Figure 3-3: Probability distribution of fluxes for $\sigma = .2$, linear binning. Solid line represents linear binned probability distribution predicted from the macroscopic model

version (2.14). Since

$$\frac{j_w}{j_a} \sim \frac{s\kappa c}{s\kappa c_a} \tag{3.16}$$

$$\log_{10}(\min(j_w/j_a)) \sim \beta(r_b - a) \tag{3.17}$$

$$\sim \beta r_b \tag{3.18}$$

the microscopic and macroscopic results in figure 3-4 are rescaled by βr_b. Only the macroscopic result for $\sigma = .2$ is shown to reduce clutter.

The macroscopic line is above the microscopic data since it assumes flux is distributed equally everywhere at distance r from the center and therefore not capturing low flux stochasticity. Both pdfs integrate to 1 so the macroscopic data is above the microscopic data.

3.2.3 Discussion

The histogram analysis was performed here to understand how diffusion limited reaction rates are distributed for the case of an absorbing porous medium.

Because of the fluctuations at all scales, we know that at least part of the medium at a distance r from the source has flux $j_w(r)$, but the scaling of the flux for other zones the same distance r away should be determined.

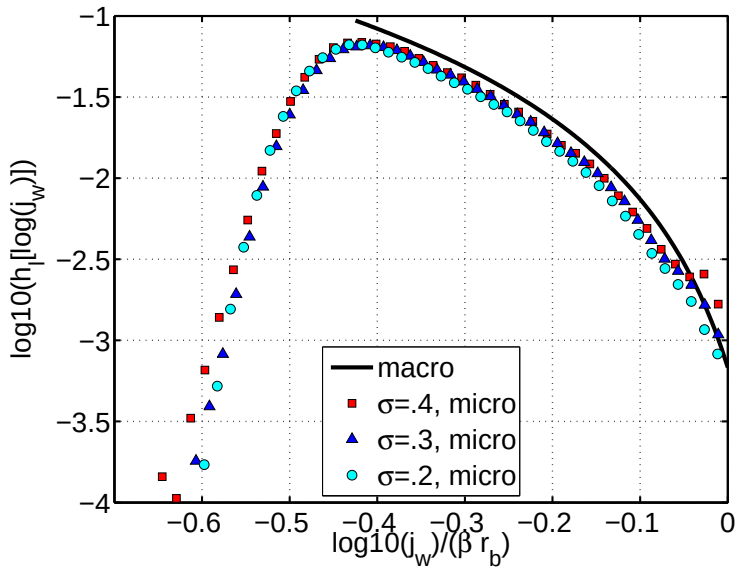

Figure 3-4: Normalized probability distribution of fluxes for various σ, log-binned. The solid line shows a normalized log-binned histogram predicted from the macroscopic model for $\sigma = .2$

The microscopic and macroscopic models compliment each other very well. Insight to the behavior of the microscopic model comes from the parameter β, which sets a critical length scale. Exactly how β relates to the microscopic geometry is discussed in the next chapter.

$p(r)$ can also be found when sources are randomly placed with number density n. The probability, P_1, that two microbes are spaced a distance $< 2r$ from each other can be determined from a Poisson point process and is $P_1(r) = 1 - e^{-4\pi n r^3/3}$. [9] This of course results in a slightly different density function than $h(j_w)$ but variations away from $1/j_w$ remain negligible. This was not discussed in depth here because the main purpose here is to compare the microscopic and macroscopic models(fixed r_b). Again, microbial decay implementations of this model are discussed in [25].

Chapter 4

Connecting the Scales

The importance of the parameter β was shown in chapter 3. There should also be some physical intuition regarding β at this point as well. For instance, if κ is thought of as an averaged absorption frequency, $\kappa = 1/\tau$, then $\beta = 1/\tau\bar{D} = 1/\delta^2$, where δ is an averaged diffusion length traveled over time τ. β^{-1} should also be directly related to l and β has been found to increase with σ.

4.1 Finding β

Consider conservation of flux in a small volume of size $\Delta V \gg l^3$, l being a typical pore size. The total flux to the surfaces in the microscopic model must be the same as the total absorbed flux in the macroscopic model.

$$\kappa c \Delta V = \int_S D \nabla C(\mathbf{x}) \cdot \mathbf{n} dA \tag{4.1}$$

Averaging the right hand side of (4.1) over all surfaces in ΔV gives

$$\kappa c \Delta V = D \langle |\nabla C| \rangle \Delta A \tag{4.2a}$$

$$\kappa c = D \langle |\nabla C| \rangle s \tag{4.2b}$$

$$\beta^2 c = \frac{D}{\bar{D}} \langle |\nabla C| \rangle s \tag{4.2c}$$

Where ΔA is the surface area in ΔV and $s = \Delta A / \Delta V$. $\nabla C \cdot \mathbf{n} = |\nabla C|$ at a surface with constant Dirichlet boundary condition.

Because $C(\mathbf{x})$ is harmonic, smooth and well behaved in the pore space we can expect $|\nabla C| \sim C/l_l$, l_l being the local pore size and $l = \langle l_l \rangle$ in ΔV. This follows from the intermediate value theorem. There is a set of points $\mathbf{x}^*$ in a pore where $C(\mathbf{x}^*) = \bar{C}$, $\bar{C}$ being the average concentration in the pore. $d^*(\mathbf{x}^*)$ is the distance from $\mathbf{x}^*$ to the nearest wall. A specific wall location is a distance $\in d^*$ from the closest point in x^*. Thus the gradient at that wall location can be approximated by $\bar{C}/d^*$ to $O(d^{*3})$ since on walls $\nabla C \cdot \mathbf{n} = |\nabla C|$ and $|\nabla C|$ is flat. Since $d^* \sim l_l/2$,

$$\langle |\nabla C| \rangle \sim \langle 2C/l_l \rangle \tag{4.3}$$

where the brackets on the left hand side of approximation (4.3) represent surface averaging and the brackets on the r.h.s. represent volume averaging in the pore space. Using this analysis,

$$\beta^2 c \sim \frac{D}{\bar{D}} \left\langle \frac{C}{l_l/2} \right\rangle s \tag{4.4}$$

$$\beta^2 c \sim \frac{D}{\bar{D}} \left(\frac{\langle C \rangle}{\langle l_l/2 \rangle} + Cov(C, l_l^{-1}) \right) s \tag{4.5}$$

C, l might be correlated since larger pores allow for higher concentrations, but there are many reasons to expect C, l to be uncorrelated in a random medium. The main reason is that concentrations in two pores an equal distance from the source may be order of magnitudes different if one of the paths is slightly more tortuous than the other as seen in figures 2-2 and D-1.

Incorporating $c = \langle C \rangle \phi$ finally gives the relation between β and the porous geometry.

$$\beta^2 \sim \frac{D}{\bar{D}} \frac{2s}{\phi l} \tag{4.6}$$

The proportionality constant comes from the gradient estimate and is geometry dependent. In most porous media s sets the length l and $l \sim 1/s$, so $\beta^2 \sim s^2$. (4.6) is a general result that should hold true for many geometries.

4.2 β Analysis for the Cubic Model

Further analysis can be done for a porous geometry consisting of randomly placed cubes of fixed size l_g. This geometry is very simple as it only contains one parameter, ϕ. [1]

4.2.1 Specific surface area

The point-point correlation function $S_2(r)$ can be used to express the specific surface area in terms of ϕ. For a digitized medium,

$$\frac{d}{dr}S_r(r)|_{r=0} = -s/2D \tag{4.7}$$

where D is the dimension of the system[37]. It is easy to argue that $S_2(r)$ should drop from ϕ to ϕ^2 over about one grain length, l_g. A numerical investigation revealed that the de-correlation distance in our simple cubic model is actually $\approx l_g/2$. Thus

$$s = 6\frac{\phi(1-\phi)}{l_g/2} \tag{4.8}$$

4.2.2 Pore size

The pore size, l, can also be expressed in terms of ϕ. There are many ways to estimate l. One way is to get an exact solution for the distribution of pore sizes in our exact system. Another way is to utilize the equations describing the pore sizes for a general heterogeneous medium, eq. 2.84 in [32]. Another way is to use results from a simpler geometry to approximate our medium. The following sections discuss various estimates of the pore size using different methods. Note that estimates $L3, L4$ all use an overlapping medium as an approximation, $L2$ uses a low solid fraction approximation, L_1 uses a uniform cubic medium as an approximation and $L5$ considers non-overlapping cubes.

Simple geometrical estimate, L_1

In order to provide physical insight, first consider a volume containing regularly spaced cubic grains of length l_g and porosity ϕ, one can easily geometrically argue that a

[1] The size of the cubes could also be changed in the microscopic mode, but the cubic model was not able to provide s comparable to marine sediment geometries, $s \sim 1e-5$ cm for sources of size $a \sim 1\mu m$.

crude approximation to the pore size is L_1, defined as

$$\frac{L_1}{l_g} \sim \left(\frac{\phi}{1-\phi}\right)^{1/3} \tag{4.9}$$

This measurement represents the cube root of the pore volume associated with each grain rather than an actual distance between grains. It may or may not be the appropriate characteristic length.

Low solid fraction limit, L_2

The most basic analytical result is obtained if the pore size is approximated by distance from center to center of the overlapping grains rather than from surfaces of the grains. This is the same as finding the pore size in a domain consisting of randomly placed points and is a good approximation when $\sigma \ll 1$.

Consider a spherical volume with radius l and one places centers at frequency n, a number density, the probability of finding a center within the test volume is

$$P_s(l) = 1 - \exp\{-\mathcal{N} l^d\}, \qquad \mathcal{N} = c_d \sigma / l_g^d \tag{4.10}$$

where d is the dimension of the system and geometrical factor $c_d = 2, \pi$, and $4\pi/3$ for one, two and three dimensions respectively [9]. Differentiating P_s with respect to l results in the probability density function of distances between particles. Taking the mean of this involves the gamma function. Since l is a radius and in general we think of it as an effective diameter, the result is

$$L_2 = 2\langle l \rangle = 2\Gamma\left(\frac{d+1}{d}\right)\mathcal{N}^{1/d} \tag{4.11}$$

and rewriting in terms of solid fraction for overlapping cubes gives

$$\frac{L_2}{l_g} = 2\Gamma(4/3)(4\pi/3)^{-1/3}\sigma^{-1/3} \tag{4.12a}$$

$$= 1.11\sigma^{-1/3} \tag{4.12b}$$

$$\sim \sigma^{-1/3}. \tag{4.12c}$$

The scaling relation, (4.12), can also be found intuitively considering a regular grid of points, but the pre-factor cannot. Note this characteristic normalized diameter is

within the range of possible diameters on a cubic lattice with unity spacing $1 < 1.11 < \sqrt{3}$. The randomness does not seem to affect the mean value much. Remember, equation (4.12) is a good approximation for pore size, l, in the simple cubic model as $\sigma \to 0$. For larger σ, (4.9) is a better approximation, therefore (4.9) should have the same pre-factor in that limit. Using this pre-factor for spherical voids,

$$\frac{L_1}{l_g} = 1.11 \left(\frac{\phi}{\sigma}\right)^{1/3} \tag{4.13}$$

Comments on pore size approximations

L_1 is a strange measure of the pore size for many reasons. For example, assigning a spherical particle volume to each uncorrelated center will result in overlap. Therefore the number density is not simply $n = \sigma/v_s$ as used in equation (4.12), but is actually $n = \log(\phi)/v_s$ [32] where v_s is the volume of the spherical particle. Further, if one assumes these particles are fully penetrable spheres, then the actual pore size can be found. To do this, pore size means average distance from a randomly chosen point in the pore space to the nearest point on the solid-pore interface. It is not certain whether this is the specific measure of pore size that is important for our problem. That result is found in section 2.6 of Torquato [32] and doesn't match L_1 well at all.

Non-overlapping cubes, L_3

A better way of estimating pore size in our system is to consider a "reverse Poisson" problem. Here consider a cubic grid of points with spacing h. Lay down a test cube of size l^3. Note that $l^3 \geq h^3$ since volumes less than a cubic unit do not count. You can also consider laying down a reasonably shaped test volume i.e. no part of the volume is thinner than h, but in this case, l is the cube root of the test volume. As in our simple geometry, every point has a probability ϕ of being empty. Note that the measure of pore size used here is simply the cube root of the test volume.

The number of points in the test cube is $N = l^3/h^3$. Here one must make 2 assumptions. One assumption is that given a volume l^3, the number of points per unit volume is approximated by N although obviously there are locations where a test cube with side $l = 1.5h$ contains 8 points and there is a slightly shifted location where that same size test cube contains only one point. This might be a reasonable approximation for the number of points in that volume averaged over all locations. The other assumption is that number of points in the volume is a non-integer. This may be

a reasonable approximation since a pore of size l does not count if a neighboring point is solid whose center is not contained in l^3.

The probability that all N points are voids is,

$$P_{void}(l) = \phi^N = \phi^{l^3/h^3} \tag{4.14}$$

In order to get pore information out of this, use Bayes theorem; the probability that N points are voids given you are in a pore, P_l, multiplied by the probability you are in the void, ϕ, is the probability that N points are void anywhere, P_{void}.

$$P_l l = P_{void}(l)/\phi \tag{4.15}$$

$$P_l l = \phi^{(l^3/h^3-1)} \tag{4.16}$$

Note that $P_l(l)$ represents the probability that the actual pore size is greater than or equal to l. Note that this is a true cumulative distribution function, since $P_l(h) = 1$ and $P_l(\infty) = 0$ for all ϕ.

Applying standard techniques, the mean pore size is obtained

$$\langle l \rangle = \int_h^\infty 3l \frac{l^2}{h^3} e^{(\log(\phi) l^3/h^3)} dl \tag{4.17}$$

$$L_3 = \langle l \rangle = h \left(\frac{\Gamma(1/3, -\log(\phi))}{3\phi(-\log(\phi))^{1/3}} + 1 \right) \tag{4.18}$$

The incomplete Gamma function is used since we only consider $l > h$. This results in a very well behaved pore estimate which never drops below h unlike the other estimates so far.

Note that we could have also considered a perhaps better estimate of our pore size by laying down a test volume of size l^3 composed of blocks of size h. This would have used a probability mass function where volumes can only be discrete sizes and resulted in a quantitatively similar answer, however the functional form would be a series solution. I also considered an even simpler discrete pore estimate where only cubes with sides having integer multiples of h were considered. This resulted in a harsh measure of the pore size which quickly dropped to h. This estimate of l poorly predicted the experimental values of β.

Comparing sizes

To summarize, L_1 is an effective diameter of the mean volume associated with a randomly placed cubic particle with overlap; L_2 is the average spherical pore diameter for randomly placed cubes with very low solid fraction. Note that all measures drop below one particle size (or grid spacing) except for L_3. L_3 is simply the mean size of empty general test volumes placed on a cubic grid whose nodes have a probability σ of being solid.

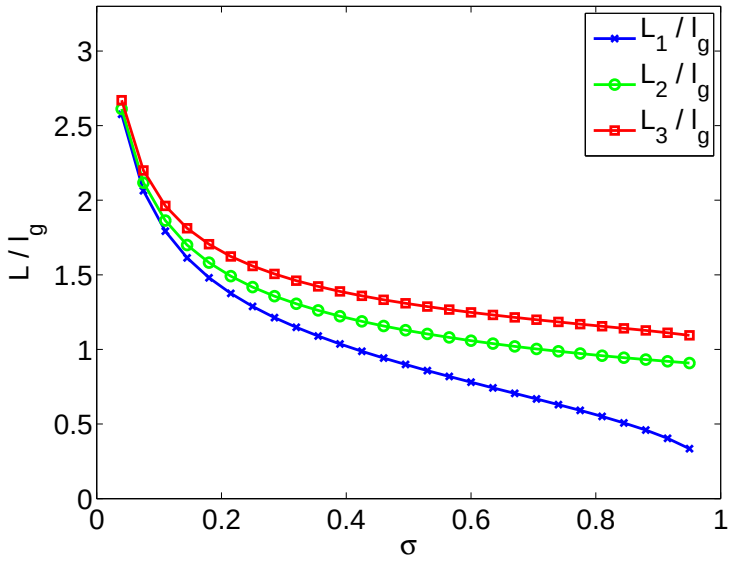

Figure 4-1: Normalized pore size L/l_g vs. σ where l_g is the size of the cubic particle which compose the medium.

Figure 4-1 shows a side by side comparison of the different measures of normalized pore size. Intuitively, L_3 should be the appropriate measure of pore size to predict β. In the figure, spherical pore sizes, L_1, L_2, are compared to the cubic pore size, L_3, via multiplication by $(\pi/6)^{1/3}$. Remember, L_2/l_g is only valid for small σ as it does not account for overlap.

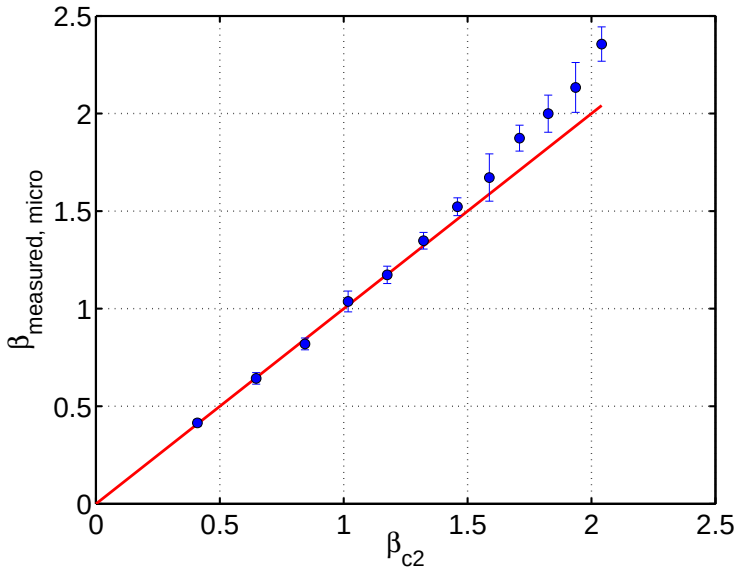

Figure 4-2: Data points are β_2 vs β determined from fitting numerical data for low σ. Each point represents a different σ, β increasing with σ. $.05 \leq \sigma \leq .6$. Solid line has slope=1. Error bars represent one standard deviation of calculations from numerical ensembles.

4.3 Comparison with Numerical Result

4.3.1 β formulation

Putting together the information about s and $l = L_2$ in conjunction with $\bar{D} = D$ from Richards with a lattice correction [22], [23] [2], allows for a rather good estimate of β for the simple cubic geometry.

$$\beta_2^2 \sim \frac{\bar{D}}{D} \frac{24\sigma^{4/3}}{1.18 l_g^2} \tag{4.19}$$

Equation (4.19) utilizes the version (4.12) formulation of l. The geometry in the microscopic model uses $l_g = 2$.

$$\beta_2 \sim 2.25\sigma^{2/3}\bar{D}/D \tag{4.20}$$

Thus β is dependent on the one geometrical parameter σ.

[2] Although $\bar{D}$ is $\bar{D}(\sigma)$, there is not much departure from the trap-free D over the range $0 < \sigma < .7$, resulting in $\bar{D} \approx D$, so I will use the *notation* $\bar{D}/D$ rather than $\bar{D}(\sigma)/D$. For all figures, β *is* fitted with the Richards relation, however this only changes the pre-factors on β by 4% compared with using $\bar{D} = D$ and changes in the plots are hardly noticeable.

To see if this analysis is reasonable, β_2 is compared with the β determined from the numerical fits in figures 4-2, 4-3. Since β_2 did not have the exact pre-factor, a pre-factor of 1.35 was determined by fitting the low solid fraction data in figure 4-2 to a slope=1. Multiplying (4.23) by 1.35 gives

$$\beta_2 = 3.0\sigma^{2/3}\bar{D}/D \tag{4.21}$$

Due to the gradient estimation (4.3), it is likely that a pre-factor of 1.35 is a coincidence. However the cubic geometries combined with the coarse discretization of the medium resulting in rough estimates of flux and pore space concentrations might make $\langle|\hat{\nabla}C|\rangle \approx \langle 2C/l\rangle$.

Finding β using other pore size estimates

Using L_1, L_3 instead, one finds similar estimates of β.

For L_1,

$$\beta_1 = 2.25\bar{D}/D\sigma^{2/3} \tag{4.22}$$

The pre-factor is the same as in eq. (4.23) since (4.9) and (4.12) are equivalent as $\sigma \to 0$. The fitted pre-factor was determined in the same way as above. Oddly, the geometry dependent fitted pre-factor is 1.31 for this better model as opposed to 1.35. This results in

$$\beta_1 = 2.95\frac{\bar{D}}{D}\frac{\sigma^{2/3}}{(1-\sigma)^{1/6}} \tag{4.23}$$

For L_3,

$$\beta_3 = \left(\frac{\bar{D}}{D}\frac{24d\sigma}{lg^2}\right)\left(\frac{\Gamma(1/3, -\log(\phi))}{3\phi(-\log(\phi))^{1/3}} + 1\right) \tag{4.24}$$

$$\beta_3 = 6\left(\frac{\bar{D}}{D}\sigma\right)\left(\frac{\Gamma(1/3, -\log(\phi))}{3\phi(-\log(\phi))^{1/3}} + 1\right), \tag{4.25}$$

where we have again used $l_g = 2$ and dimension $d = 3$. The pre-factor necessary for this estimate and used in figure 4-3 is 1.18.

Figure 4-3 shows the relation between $\beta_1, \beta_2, \beta_3$ and solid fraction.

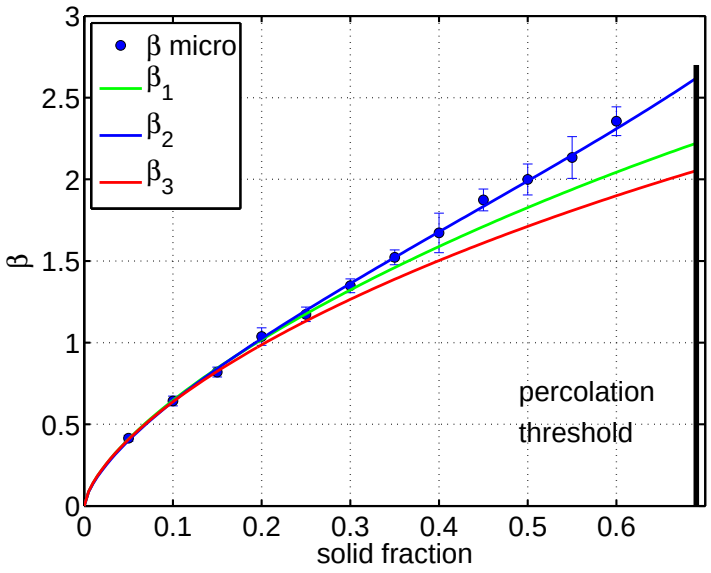

Figure 4-3: β_2 vs σ, $0.05 \leq \sigma \leq 0.6$. Points are measured β from microscopic simulations. Three lines represent β predicted from three different measures of the pore size. Vertical line at $\sigma = 0.69$ represents the percolation threshold, $\phi = p_c = 0.31$. Above this threshold, β cannot be found given our source boundary condition. Error bars represent one standard deviation.

4.3.2 Discussion

Most striking is that the pore size measurement that is supposed to most closely reflect an actual pore size yields the estimate β_3, which has the most error. Since β_1 matches best with the numerical experiment, perhaps the strange size L_1 is the length which is most appropriate to determine β in this system.

Additionally, one needs to consider the case where $\phi \to p_c$. In the literature [32], one typically considers the static trap problem with constant generation in the pore space. In that case, as percolation is approached, volumes are enclosed but there is generation in the *entire* pore space so the surface area and porosity associated with concentrations continuously approach and surpass the percolation threshold. Therefore, disconnecting the pore space does not restrict access within it so β does not exhibit critical behavior. For our case however, one might think disconnecting the pore space may have an effect, as the effective porosity and effective specific surface area should change more quickly as percolation is approached. Effective specific surface area is the actual surface area per unit volume exposed to the diffusing concentration and also the effective porosity of the medium. Effective porosity is the void fraction where concentration is non-zero or the fraction of void space which is

connected to the source. These effects should be important as our scaling model is based on both the effective porosity and effective specific surface area. Both the effective specific surface area and the effective porosity should also be smaller than the actual specific surface area and porosity. However, remember that β represents a characteristic foraging distance, and cutting off volumes to it most likely should not effect β since the foraging distance is really related only to the immediate environment. If a particle is in a pore or path, then who cares if other volumes aren't accessible anymore, its only the local pore/path properties that count.

Remember that many orders of magnitudes of concentration fluctuations are being radially averaged to get β. Therefore we are really finding the macroscopic properties of how the "safest paths" vary with microstructure. Close to percolation, there will be few paths extending from the source to the boundary. If large ensembles are run, then eventually a good path will be hit upon and that will dominate the average. Thus there may be no reason to expect to see critical behavior in κ and β even in our system with localized sources. For our numerical experiments, $p_c = 0.69$, and $\max(\sigma) = 0.6$, so we may not be close enough to percolation to notice critical phenomenon. If it is noticed, more ensembles should be taken in order to account for the sparse paths in each geometrical realization before conclusions are made.

To tackle this problem if the critical phenomena do exist, an approach would measure the effective specific surface area, $\mathcal{S}$, by counting only surfaces with non-zero gradient. This effective $\mathcal{S}$ is analogous to the dynamic length Λ in [27]. The effective porosity can be defined in the same way. Intuitively however, if we consider an effective specific surface area per unit active pore space, then is should be the same as specific surface area per unit pore space (whether the pore is active or not). Further work in these areas may give better estimates of β for the full range $0 < \sigma < p_c$.

Although it is difficult to tell, there should be error in our estimate of β as $\sigma \to 0$. This is due to our result in the low solid fraction case, $\beta^2 = 9.0\sigma^{4/3}/R^2$ where $R = l_g/2$, not matching the Smoluchowsky result $\beta^2 = 3\sigma/R^2$. The difference arises because unlike previous work finding β, κ, our model is *designed specifically to work only when trap interactions dominate.* Previous work [10], [11] starts from the Smoluchowsky model and attempt to modify it via inclusion of the effects of trap interaction. In our model at lower solid fraction, the gradient will no longer scale with the pore size l, as interactions from neighbors will not affect the flux to a single absorber. Also, the flux per wall of a pore space with size l composed of very

sparse walls is *higher* than the flux per wall of a pore space *completely surrounded by walls* with the same size and average concentration. Therefore one may expect β to be higher than our prediction as $\sigma \to 0$ as indicated when comparing our result vs. Smoluchowsky's.

4.3.3 Comparison to Previous Results

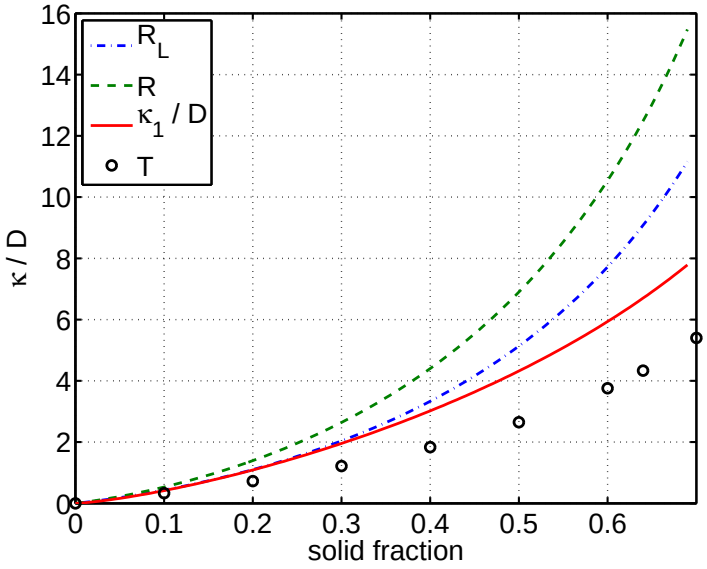

Figure 4-4: κ/D vs σ, $.05 \leq \sigma \leq .7$. Solid line is $\kappa/D = \beta_1^2 \bar{D}/D$. Line R, is eq. (7) in [22]. R_L is R with a correction from [23] accounting for lattice effects. Both results R, R_L are modified so the actual solid fraction is plotted on the x-axis. Line T comes from the table in [31] and eq. (3) in [24].

Figure 4-4 compares κ/D for known results for overlapping spheres to our result for cubes on a grid. The dotted line, denoted R, is a result from Richards [22] and is considered an upper bound for overlapping spheres. Richards obtained κ by finding survival probability as a function of time for random walkers amongst traps [23]. Taking the average of that quantity over all time gives his estimate of κ. If the spheres are placed on a lattice such that the radius of the sphere used in the random walk analysis is $\sqrt{3}$, then the sphere is actually a cube with side of length 2, just like in our simulation. The correction for this lattice effect on Richards' result is shown by R_L. Note that R_L matches our result very well for $\sigma < 0.3$ which is to be expected since Richards' solids are overlapping. The overlap effect is more pronounced at higher solid fraction, and we notice the deviation occurring for $\sigma > 0.3$. However,

the direction of the discrepancy is slightly counter-intuitive since for a fixed solid fraction, any smoothening due to overlap should result in lower specific surface area. On the other hand, the effect of exclusion of voids in my situation effectively makes for "bigger solids", and smaller specific surface area. Although hard to tell on this plot, zooming in reveals our result is less than the other results as $\sigma \to 0$ since our result in that regime is $\kappa \propto \sigma^{4/3}$ while theirs is the Smoluchowsky $\kappa \propto \sigma$. The Torquato result [31] comes from an analysis of the steady microscopic equation with constant generation in the pore space [7]. Here the $c = 0$ boundary condition on the interface is replaced by a term in the equilibrium equation involving delta functions on the surfaces. Then, after averaging the concentration the bulk absorption can be found in terms of typical parameters of the porous medium. The closed form result is complicated and is presented as a table in [31]. It is claimed to be a lower bound. Note that our non-overlapping cubic result lies between the bounds for overlapping spheres. Non-overlapping cubes coagulate more similarly to overlapping spheres than non-overlapping spheres.

My result for κ can also be compared to survival times of lattice diffusion with traps, where a trap is a single lattice site. This problem in 3D has been well studied by Anlauf whose results are discussed by Mehra and Grassberger, [16], and Barkema, Biswas, and van Beijeren [2]. The lattice problem has received attention more recently than the continuous problem, with the two dimensional problem being fully addressed in 2001 [12]. The problem with using lattice results for our system is that we actually have a mix of correlated and random traps since we lay traps down in the form of cubes with 3 sites per edge. Again, my geometry is laying spheres on a grid with a radius between 2 and $\sqrt{3}$ grid spacings, and it would make more sense to compare that to Richard's result with lattice correction. Ziff [38] found that for a simple cubic (SC) lattice model, the effective radius of the absorbers is $\approx .31a$, where a is a grid spacing. I visually compared survival times from Anlauf's lattice result to the Richards result with lattice correction and found setting the radius to $.24a$ in Richard's model best matched Anlauf's scaling. Therefore, these two problems are related, but when I place solids of length 2 on the grid, comparison of our result with the SC lattice result is difficult since for moderate solid fraction, channels in my medium may have unity width but length 3. Also, the discussion of continuous problem tends to include physical properties of porous media while discussions of the lattice problem do not involve concepts like specific surface area.

Chapter 5

Quasi-Steady Monte Carlo Model

There are certain properties of the models presented in chapters 2 and 3 that are counterintuitive (but not necessarily unrealistic) when trying to model enzymatic degradation of organic carbon. One such property is that the distribution of reaction rates remains in the same initial configuration after long time, even though the carbon on surfaces with high fluxes is wiped out. This is due to the assumed boundary conditions and is related to the other perhaps unrealistic properties of the model mentioned in section 2.1. This Monte-Carlo model tries to address some of those issues, but in the end it turns out to be of less interest than we originally hoped.

5.1 Description

At the heart of this model is the Gillespie method [13]. The model considers reactions to be taking place on walls. Walls are considered to be either completely covered with food, $C = 0$, or depleted, $\nabla \mathbf{C} \cdot \mathbf{n} = 0$. At time $t = t_0$, all walls are covered and the steady state solution to (1.1)- (1.3) is computed. At time $t^i = t^{i-1} + \Delta t^i$, one wall is randomly switched from absorbing to reflecting. This quasi-steady process can be iterated until a desired amount of carbon has been eaten.

Since reactions on walls are a Poisson process, the time between the i^{th} and $i^{th}+1$ reaction is the probability distribution

$$\Delta t^i = -/log(q)/\Sigma_j k_j^i, q \in U[0,1] \tag{5.1}$$

where $\Sigma_j k_j^i$ is the sum of all reaction rates at time t^i. Diffusion limitation assumption states the distribution $k^i \propto \{j_w\}^i$. The probability that the j^{th} boundary is chosen

at time t^i is

$$\mathcal{P}_j = k_j / \Sigma k_j. \tag{5.2}$$

Because of the weighting on this distribution, the walls closest to the source are picked first and the depletion moves as a spherical front with radius $R(t)$.

5.2 Results

Due to conservation of flux, $\Sigma k^i = I_a / c_c, \forall i$, where I_a is the total flux emitted from a source of radius a and c_c is a concentration conversion factor.

$$\Delta t^i = -/log(q) c_c / I_a \tag{5.3}$$

$$\langle \Delta t^i \rangle = 1/(I_a/c_c) \tag{5.4}$$

Thus, the time step is roughly constant with small variation.

Because the system is assumed to be quasi-steady and reactions are diffusion limited, the depletion front dynamics on the simple cubic geometry are

$$R^3(t) = \frac{3}{24\pi} \frac{l_g^3}{\sigma} \frac{I_a}{c_c} t \tag{5.5}$$

$$R(t) \propto t^{1/3} \tag{5.6}$$

Figure 5-1 shows the depletion front does indeed move with $t^{1/3}$. The reaction rate, k at distance R is $k \propto R^{-3}$. Using the same statistical analysis as in the previous chapters, the probability density of k is

$$P_k \propto k^{-2} \tag{5.7}$$

This distribution seems well behaved since there is a finite size of material, $R \leq R_b$, resulting in $min(k) > 0$. But regardless, constancy of the time step results in reactions that degrade the enviroment at a constant rate; $\dot{g}$ is constant where g is the amount of carbon left in the system. To compare to a first order system, the overall reaction

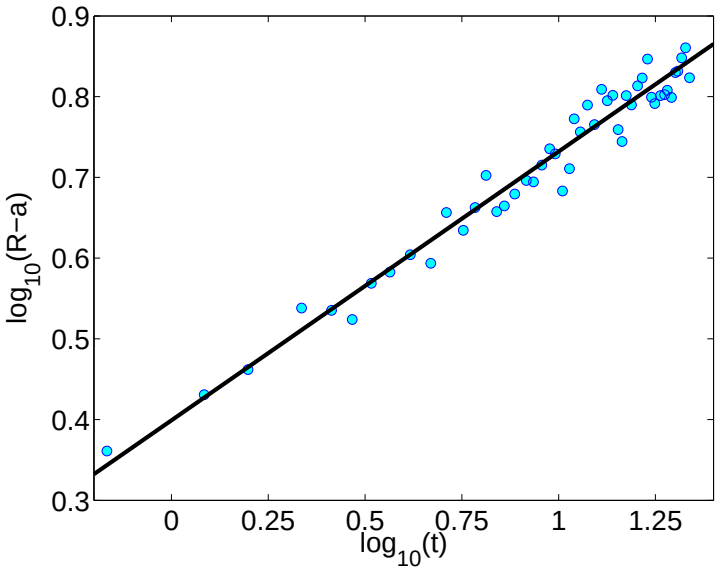

Figure 5-1: $R - a$ vs. t. Monte-Carlo simulation. R is in grid units. The solid line has slope $= 1/3$

rate is $K = \dot{g}/g$, resulting in (5.4),

$$g = g_0 - \alpha t \tag{5.8a}$$

$$K = \frac{\alpha}{g_0 - \alpha t}, \quad \alpha t \leq g_0. \tag{5.8b}$$

Since it is immediately seen that overall reactions do not proceed as the geologically measured rate $K \sim 1/t$ [17], we decided that this model did not have high priority in the near future.

Chapter 6

Concluding Remarks

6.1 Summary

Models for diffusion through porous media have been proposed on two different length scales. The models have been found to complement each other and provide insight into the behavior of porous media absorption. Most of the analysis performed requires that the product of a typical particle foraging distance β be much less than the distance from source. This results in a concentration which decays exponentially with distance. Absorption in the bulk is characterized by β^2 and has been found to be a function of geometrical parameters. β for the simple cubic model has been found to scale with $\sigma^{2/3}$. Our result for bulk absorption is much simpler and more physically intuitive than previously published results. However, our scaling result is only good for a moderate range of σ which is more appropriate for reactions in porous media rather than general homogeneous diffusion limited reaction. Another new contribution is finding that absorption fluxes, j_w, vary with distance r from the source like $j_w \sim \exp \beta r$ and the harmonic measure of j_w was found to be $\sim j_w^{-1}$. This model and the results presented here inspired the model and work done in [25].

As discussed in section 3.1, appendix D and [30] fluctuations at all scales may have implications for the actual absorption per unit volume, and further work should be done here to determine the acutal implications of this on our bulk properties, flux results $\jmath_w$ and how these fluctuations can affect overall reaction rates.

6.2 Relation to the Physical Decay Problem

This thesis model may not directly apply to the biodegradation problem since it requires many assumptions.

The first, as mentioned in the introduction, is that enzymes are catalysts and are not consumed in the reaction or known to stick to clay. The $C = 0$ interface boundary condition requires these assumptions or something similar which results in absorption. As mentioned in section 2.1, large molecular weight polymers, of similar weight to many enzymes, adsorb to minerals rather readily and it is not clear whether this boundary condition is appropriate or not. Regarding the possibility of first contact with a substrate denaturing the enzyme, intuition tells us that frequent hydrolysis give the enzyme more chances to denature as interacting molecular forces disturb the enzyme from its equillibrium state. An enzyme working locally on one section of substrate may denature before it gets to another area. Enzymes may also have a characteristic "lifetime" before they denature depending on the environment [34]. This lifetime may be different while adsorbed to clay or the substrate, or maybe enzyme denaturation is just as likely in the pore space as anywhere else. In [25], we use a different microscopic model where interfaces are reflecting and the reaction diffusion equation governs the concentration in the pore space. The macroscopic model is the same as presented here, but β is based on effective diffusion and enzyme lifetime. κ is dependent on geometrical parameters very similar to those discussed in this thesis.

Another conflict with real systems is we assume all surfaces are the same. In reality, only a fraction of carbon surfaces are associated with POC and another fraction are exposed minerals. Some of these may be reflecting, absorbing, radiative, or saturating. To address part of this problem, the effective diffusion coefficient $\bar{D}$ will need to be accounted for in addition to effects on the absorption coefficient, κ, if we assume the mineral surfaces reflect rather than adsorb the enzyme. The same issue occurs however when the microscopic model has all reflecting interfaces.

Perhaps the most questionable assumption in applying the model to biodegradation problems is that we assume the flux of enzymes from the microbe is constant during the burial process. This may be unrealistic from energy balance considerations since this model also assumes a microbe's environment is continually degrading [34]. However, it is consistent with the finding that there seems to be a decent amount of DOC being emitted from the ocean floor [5]. Perhaps microbes need only a small

concentration of low molecular weight DOC to survive and are living in a surplus of DOC. In this case, it may suggest that a bug steadily releasing enzymes in a surplus may be simply inefficient, or perhaps it wishes to break down the high molecular weight DOC near to it. The question that now arises is how long (deep) does that surplus last? Burdige [4] proposes that there is a small generation of DOC even at deeper depths, and that's why measured DOC concentrations remain constant at deeper depths. For many conditions, the DOC concentration horizon is on the order of the maximum concentration in the profile. Therefore it seems as if this surplus is somehow sustained, and the validity of the constant source flux assumption is unclear.

6.3 Future Aspirations

Proper expansion of the model may lead to a major step forward to eventually reach a generic model for organic matter degradation and burial in ocean sediments and perhaps even soils.

There are many future biological directions this work can take. Some have already been initially investigated by Vetter et al. [34]. Ideally, one would simply like to estimate the effect that additional realistic mechanisms would have on the reaction rates determined from simple model proposed in this thesis and in [25].

- Accounting for microbial flux response to a continually degrading environment.
- Possible extension of these ideas to model degradation in surface soils.
- Model the return process of food to the microbe.
- Couple the return process with microbial response to make a model of bacterial growth.
- Understand enzyme behavior and enzymatic hydrolysis further and use this information in our model.
- Expand upon this model to account for boundary conditions which allow for more realistic chemistry, most likely involving a coupled OC reaction model. It would be interesting to see how the more "realistic" chemistry model changes the rate distribution.

- Make a model which has two scales of clay geometry resulting in regions with different $\bar{D}$. This may address more realistically where POC globules are hiding. This is more realistic physically.

- Addressing more realistic geometrical boundaries of clay and POC.

Although it is very enticing to attempt to tackle the problem of carbon burial, there are many purely physical aspects of this model that are also interesting. They include

- Finding the effect of the concentration fluctuations on bulk properties and fluxes as well as how this affects the overall reaction rate.

- Figure out how the "safest paths" are varying smoothly with geometrical changes and why exactly did our scaling analysis predict β so well if it is really the "safest paths" that are governing averaged concentrations.

- Investigate the mapping of the paths to the maximum concentrations, and find if any interesting dynamics are occuring.

- Finding the effect of partially covered clays on β.

- Determine how approaching the percolation threshold affects β for our case when generation comes from a local source.

- Find β for other specific geometries, from basic geometries to those of flat platelets similar to clays in sediment.

  - Find β for 2-D systems and compare with our numerical 2-D results.
  - Find the implications of connected geometries.

- Do all of the above for the reflecting boundary model with uniform reaction in the bulk.

- Understand β from a random walker perspective rather than a microscopic prospective. Develop a model for travel based on hitting a wall in the next step.

- Further analysis of the histogram turnover and perhaps how it relates to the work of Duplantier[8].

- Studying the peculiarities of the decoupling effect in the numerical simulations.
- Analyze how various boundary *conditions* may affect the reaction rates and results in general.
- Figure out exactly which geometric properties determine κ for the case of microscopic reflecting boundaries.

Applying the general model presented here to the other physical problems mentioned in the introduction may also be done.

Due to the richness of this problem, the next step should be exciting regardless of the direction I take. I am very fortunate to be a part of it.

Appendix A

Table of Parameters

Symbol	Description	Typical values Nature	3-D Simulation
a	microbe radius	5×10^{-5} cm	1 gu
j_a	enzyme source flux	10^{-10} g s^{-1} cm^{-2}	1 g s^{-1} gu^{-2}
l_g	size of single grain	10^5 cm [a]	2 gu
D	molecular diffusivity	10^{-7} cm^{2}s^{-1}	1
β	typical foraging distance	$10^{-5/2}$ $\bar{D}^{1/2}$m [b]	~ 2 gu
r_b	typical microbe spacing	10^{-2} cm [c]	32 gu
s	specific surface area	10^6cm^{-1}[14],[34]	3σ gu^{-1}
l	typical pore size	10^{-6}cm [d]	varies
σ	solid volume fraction	$.1 < \sigma < .3, +/- .1$ [e]	$.05 \leq \sigma \leq .6$
C	pore space concentration		
c	macroscopic concentration [f]		
j_w	absorptive flux to walls		
H	pdf of j_w, microscopic		
H_l	pdf of $log(j_w)$, microscopic		
h	pdf of j_w, macroscopic		
h_l	pdf of $log(j_w)$, macroscopic		
κ	bulk absorption coefficient		

Table A.1: Typical values of parameters, Note that the value for j_a is a maximum. Unit gu stands for grid units. Typical values found in nature are also presented here just as a reference. The numerical model presented here does not attempt to model natural processes.

[a] $l_g \sim 1/s_g$, s_g is surface to volume ratio of single grain $\sim 10^5$ cm^{-1}[34]
[b] $\beta \sim \sqrt{\bar{D}/\alpha}$, α is characteristic enzyme inactivity rate from [34].
[c] $r_b \sim n^{-1/3}$, n is bacterial count per unit volume $\sim 10^{-6}$cm^{-3} [26].
[d] $l \sim 1/s$
[e] values typical for upper meter of most marine sediment[4].
[f] $c = C\phi$

Appendix B

Comments on Numerical Solution

B.1 Accuracy of Numerical Solution

The 2-D and 3-D microscopic problems have been stated as equations (1.1)- (1.3), but since they are treated numerically, the problems solved here are actually,

$$\hat{\nabla}\hat{\mathbf{C}} = 0, \tag{B.1}$$

With the corresponding discrete boundary conditions. $\hat{\mathbf{C}}$ is a vector whose elements, $\hat{C}_j$ represent the concentration at node j located at $\hat{\mathbf{x}}_\mathbf{j}$. $\hat{\nabla}$ is the discrete Laplacian operator and is defined differently for finite-element and finite-difference methods. In the 3-D microscopic model used, the discretization was coarse, with the discretization step, h, being only half a grain size.

One may wonder why we expect good results from a coarse approximation to the original problem we proposed (1.1)-(1.3). A nice answer to this question is to say, we are not originally trying to solve Laplace's equation. We are attempting to solve a random walk problem, which in the continuum limit is Laplace's equation. Our coarse approximation is simply a random walk model which is a very simple approximation of the physical problem we wish to tackle.

If one is curious about how the solution to our model differs from the solution to a more realistic random walk model, $h \to 0$, it is addressed in the following way. The exact solution to (B.1) differs from the solution to equation (1.1) at $\hat{\mathbf{x}}_j$ by a discretization error, e_j. The discretization error for both the 3-D finite difference 7 point stencil and for the the finite element method used is of order h^2. For the finite

difference method used,

$$A\mathbf{e} = \mathbf{r} \tag{B.2}$$

where A is the Gauss-Seidel operator and

$$r_i = \frac{h^2}{12}(C_{xxxx}(x_i + \Theta h, y_i, z_i) + C_{yyyy}(x_i, y_i + \Theta h, z_i) + C_{zzzz}(x_i, y_i, z_i + \Theta h)), \tag{B.3}$$

where $\Theta \in [-1, 1]$[33]. Since A^{-1} is bounded and knowing that the concentration quickly dissipates for these systems, only order of magnitude knowledge of concentrations is necessary. Therefore error due to a coarse discretization is insignificant for our purposes. Note that the simplest model would have been a node-grain model, where each node represents a single grain. Future work may consider this model. A similar argument can be made regarding the accuracy of the 2D results.

B.2 Rapid Convergence of Gauss-Seidel

For an elliptic PDE discretized on an NxNxN grid, the Gauss-Seidel method requires $O(N^5)$ operations ($O(N^2)$ iterations) for a solution. Successive Overrelaxation and Multigrid methods require $O(N^4)$ and $O(N^3)$ operations respectively [21]. Therefore Gauss-Seidel is usually not implemented. However, for our problem, we noticed that the convergence of Gauss-Seidel was much faster than $O(N^2)$ iterations. The random Dirichlet boundary conditions seem to have effectively decoupled the system into smaller sub-domains requiring very few iterations to reach the desired precision. When scaling the problem up from a 32x32x32 grid to a 256x256x256 grid, with the same solid fraction, the number of iterations required went like $O(N/2)$, as information only had to travel from the center to the edge. This effect was not as strong for high porosity, as each sub-domain was rather large.

It appeared to me that the number of iterations required for convergence was roughly $O(max(N, n^3))$, where n is the size of the largest sub-domain. Most of the solid fractions in the range $.05 < \sigma < .45$ resulted in very small sub-domains compared to N so the number of iterations required for our model went like $O(N^4/2)$, although more iterations were required for $\sigma = .05, .1$. Due to this decoupling effect, SOR would likely provide no additional advantage other than maybe a factor of 2. The

extra effort for implementing a multigrid method for this type of problem might be worth it only if we were going to analyze only 256x256x256 systems or higher, but the 64^3 system gave smooth enough results and 256^3 is where even $O(N^3)$ begins to beckon for parallel processing.

Gauss-Seidel could be a fast algorithm for any elliptic PDE with the condition that Dirichlet boundary conditions be distributed frequently throughout the domain. When geometries with reflecting boundaries are eventually considered, multigrid methods will be used.

Appendix C

Effective Diffusion Coefficient in a Purely Absorptive Environment

Identifying the effective diffusion coefficient, $\bar{D}$, in porous media is an old problem. *Maxwell's law of mixtures (1881)* states the effective resistivity of a medium composed of a mixture of two phases with different conductivities. The effective diffusivity has been found as a function of many characteristic geometrical parameters including the tortuosity. The thermal conductivity of random media and even fractals has been studied.

There is one problem with all of this information about $\bar{D}$. Standard estimates of $\bar{D}$ deal with porous media where the solid phase is less penetrable than the pore space, most of the time acting as impenetrable, reflecting obstacles. $\bar{D}$ for a purely absorbing porous medium is a different subject.

A physical interpretation of $\bar{D}$ in absorbing media can be stated in the following manner. Since molecules are absorbed at first contact with a solid surface, any molecule in the pore space has not encountered a boundary and is not aware of the boundary's presence. Intuitively, the particles still alive are diffusing normally. Therefore boundaries play a role in reaction but do not seem to directly affect diffusion, so we should expect $\bar{D} \approx D$. Interactions with the solid boundaries are taken into account macroscopically by the absorbing term rather than the diffusion term.

However many others have found that $\bar{D} \neq D$, although it is close. Departures from D at very low solid fraction are found to first order in [10], [3], but as solid fraction increases slightly more, it tends to level off, [19], [6]. The perhaps even better result from Richards, [22], shows a very small monotonic increase in $\bar{D}(\sigma)/D$

from $\bar{D}(0)/D = 1$ for overlapping spheres, to $\bar{D}(.7)/D = 1.1$. Curiously, all estimates of $\bar{D}(\sigma)$, show an increasing diffusion coefficient as solid fractions increase but overall, $\bar{D}(\sigma)$ is rather insensitive to changes in solid fraction.

A physical reason for this accelerated diffusion coefficient is hard to come by. Part of the problem is that randomly walking particles in the void space are not encountering traps in a purely poisson process. Randomly walking particles have a *memory* of where they've been. Therefore after t time steps, active particles which randomly stay in the same neighborhood have good chance of encountering previously visited "safe" sites which aren't traps. Particles which are more adventurous on the other hand, encounter many new unknown sites and are more likely to not survive t time steps. Therefore there is a bias towards particles which stay closer to the source. Defining D_s as the typical mean-square measure of a diffusion coefficient, it is found that $D_s < D$ [22] which agrees with this memory bias. Unfortunately, in our steady state problem $\bar{D} \neq D_s$. A physical interperetation of $\bar{D}$ comes from looking at diffusion from the absorbing material's perspective. Since absorption is more likely if a particle travels further after a given time, the material thinks that slightly more particles are reaching that area than if it was pure *poisson* absorption. Therefore, the absorbing material thinks diffusion is accelerated, when in reality, survival probability is a function of space and it is more likely that survivors further away will be absorbed in the next time step.

Alternatively, look at it from a particle point of view; consider a source with a fixed concentration. There will be a steady state particle distribution in space. Move one time step forward in steady state. Determine the number of particles absorbed as a function of distance; of course this decreases with distance simply because number of particles decreases with distance. Because of memory however, there will be a higher steady state concentration closer to the source than in the pure poisson case (no memory, $\bar{D} = D_s$). Therefore you would expect more particles to diffuse over to the next region, and this process continues further out although memory decreases with distance as well. So not only does this memory effect change the concentration gradient, but the memory effect is less as you move further away. This is what changes the diffusion coefficient. A region slightly closer to the source may have more particles with memory than the next, so this means that transport is favored slightly more away from the source. Therefore, when the particle moves to the next region, it is not equally likely to move back as it was to move there. Heres the kicker: in regular

diffusion, if there is a concentration gradient across a plane, particles randomly walk across the plane from both sides proportional to the local concentration, but since there is a gradient in concentration, this gives a net flux. In this case with absorbers, there is a concentration gradient with a source to the left of the plane, but they are not as likely to move from right to left as they are left to right. This results in accelerated diffusion away from the source. See [22] for a more concise reason.

Another way to think of it is through the continuous microscopic system. Because there are pores, concentrations can build in pore spaces compared to a purely poisson system where the boundaries are randomly varying with same porosity. The concentration build up in pore spaces is the memory effect, rewarding particles who stay in one place. Any gradient in concentration represents straying from the neighborhood and taking more chances to meet an absorber.

Appendix D

Low Flux Stochasticity

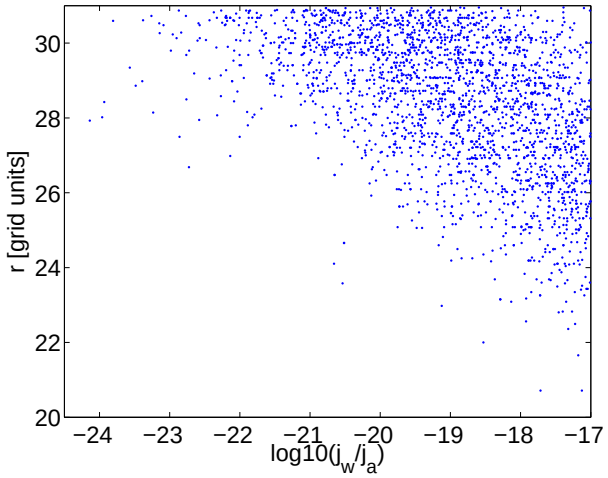

Figure D-1: Distance from source vs j_w/j_a. The points shown here are sampled from a single geometry with $\sigma = 0.3$.

The histograms in figures 2-4, 2-6, and 2-7 show a drop-off for the low fluxes. To find spatially where the tail is located, only locations with flux lower than the turnover flux were sampled. The distance from the source is compared with the flux in figure D-1. This figure explains a lot. The macroscopic histogram can be estimated from this figure by finding the average flux distribution for each r. Since the radial average used was linear, $r = 31$ should have an average flux of around 10^{-18}, corresponding with the location of the turnover for $\sigma = 0.3$ in figure 2-6. It was noticed in both the 2D and 3D simulations that the tail did not vanish as the system size increased. To explain, the distribution holding r constant spreads over many of magnitude. The tail width is roughly $\Delta j_w = \max(j_w|_{r_b}) - \min(j_w|_{r_b})$. Δj_w occurs due to the distribution of possible paths from the source to $r = r_b$. The number of paths most likely increases

with r_b^D, D being system size, and this might have to do with the scaling of the tail. These fluctuations are the fluctuations discussed by Tokuyama and Cukier in [30]. For each distance from the source, there is a path of least resistance associated with it. Each distance does not necessarily have the same path. What is measured when averaging is the concentration at the end of each path. The full implications of this on the bulk properties of our medium are unclear. Additionally, mapping the locations of the max concentrations allows the geometries of these safe areas to be seen. This could provide insight to the problem and answer questions such as what is required for the safest areas to be connected, what causes the termination/start of safe areas if they are indeed flucutating with distance, and what can a macroscopic view of this type medium actually tell us.

Bibliography

[1] Farooq Azam. Microbial control of oceanic carbon flux: the plot thickens. *Science*, 280:694–696, 1998.

[2] GT Barkema, P. Biswas, and H. van Beijeren. Diffusion with Random Distribution of Static Traps. *Physical Review Letters*, 87(17):170601, 2001.

[3] M. Bixon and R. Zwanzig. Diffusion in a medium with static traps. *The Journal of Chemical Physics*, 75:2354, 1981.

[4] David J. Burdige. *Geochemistry of Marine Sediments*. Princeton University Press, first edition, 2006.

[5] D.J. Burdige, W.M. Berelson, K.H. Coale, J. McManus, and K.S. Johnson. Fluxes of dissolved organic carbon from California continental margin sediments. *Geochim. Cosmochim. Acta*, 63(10):1507–1515, 1999.

[6] RI Cukier and K.F. Freed. Diffusion controlled processes among stationary reactive sinks: Effective medium approach. *The Journal of Chemical Physics*, 78:2573, 1983.

[7] M. Doi. A new variational approach to the diffusion and the flow problem in porous media. *J. Phys. Soc. Japan*, 40:567–572, 1976.

[8] Bertrand Duplantier. Harmonic measure exponents for two-dimensional percolation. *Phys. Rev. Lett.*, 82(20):3940–3943, May 1999.

[9] Jens Feder. Flow in porous media. personal notes, Oslo, Norway, 1996.

[10] BU Felderhof and JM Deutch. Concentration dependence of the rate of diffusion-controlled reactions. *The Journal of Chemical Physics*, 64:4551, 1976.

[11] M. Fixman. Absorption by static traps: Initial-value and steady-state problems. *The Journal of Chemical Physics*, 81:3666, 1984.

[12] L.K. Gallos, P. Argyrakis, and K.W. Kehr. Trapping and survival probability in two dimensions. *Physical Review E*, 63(2):21104, 2001.

[13] Daniel T. Gillespie. A general method for numerically simulating the stochastic time evolution of coupled chemical reactions. *Journal of Computational Physics*, 22:403–434, 1976.

[14] J. I. Hedges and R. G. Keil. Sedimentary organic matter preservation: an assesment and speculative analysis. *Marine Chemistry*, 49:81–115, 1995.

[15] L. M. Mayer. Relationships between mineral surfaces and organic-carbon concentrations in soils and sediments. *Chemical Geology*, 114:347–363, 1994.

[16] V. Mehra and P. Grassberger. Transition to Localization of Biased Walkers in a Randomly Absorbing Enviroment. *Arxiv preprint cond-mat/0107525*, 2001.

[17] J. J. Middleburg. A simple rate model for organic matter decomposition in marine sediments. *Geochemica et Cosmochimica Acta*, 53:1577–1581, 1989.

[18] Michael B. Monagan, Keith O. Geddes, K. Michael Heal, George Labahn, Stefan M. Vorkoetter, James McCarron, and Paul DeMarco. *Maple 10 Programming Guide*. Maplesoft, Waterloo ON, Canada, 2005.

[19] M. Muthukumar. Concentration dependence of diffusion controlled processes among static traps. *The Journal of Chemical Physics*, 76:2667, 1982.

[20] RL Parfitt and DJ Greenland. The adsorption of poly (ethylene glycols) on clay minerals. *Clay Minerals*, 8(3):305–315, 1970.

[21] William H. Press, Saul A. Teukolsky, William T. Vetterling, and Brian P. Flannery. *Numerical Recipes in Fortran 77*. Cambridge University Press, second edition, 1992.

[22] P.M. Richards. Diffusion and trapping at arbitrary trap size and concentration. *The Journal of Chemical Physics*, 85:3520, 1986.

[23] P.M. Richards. Diffusion to Finite-Size Traps. *Physical Review Letters*, 56(17):1838–1841, 1986.

[24] P.M. Richards and S. Torquato. Upper and lower bounds for the rate of diffusion-controlled reactions. *The Journal of Chemical Physics*, 87:4612, 1987.

[25] D. Rothman and D. Forney. Physical model for the decay and preservation of marine organic carbon. *Science*, 316(5829), 2007.

[26] J. L. Schmidt, J. W. Deming, P. A. Jumars, and R. G. Keil. Constancy of bacterial abundance in surficial marine sediments. *Limnology and Oceanography*, 43:976–982, 1998.

[27] L. M. Schwartz, N. Martys, D. P Bentz, E. J. Garboczi, and S. Torquato. Cross-property relations and permeability estimation in model porous-media. *Physical Review E*, 48:4584–4591, 1993.

[28] Dietrich Stauffer. *Introduction to Percolation Theory*. Taylor and Francis, first edition, 1985.

[29] AD STEEN, C. ARNOSTI, L. NESS, and NV BLOUGH. Electron paramagnetic resonance spectroscopy as a novel approach to measure macromolecule-surface interactions and activities of extracellular enzymes. *Marine chemistry*, 101(3-4):266–276, 2006.

[30] M. Tokuyama and R.I. Cukier. Dynamics of diffusion-controlled reactions among stationary sinks: Scaling expansion approach. *The Journal of Chemical Physics*, 76:6202, 1982.

[31] S. Torquato. Concentration dependence of diffusion-controlled reactions among static reactive sinks. *The Journal of Chemical Physics*, 85:7178, 1986.

[32] S. Torquato. *Random Heterogeneous Materials: Microstructure and Macroscopic Properties*. Springer, 2002.

[33] Alsak Tveito and Ragnar Winther. *Introduction to Partial Differential Equations A Computational Approach*. Texts in Applied Mathematics. Springer, first, second printing edition, 2005.

[34] Y. Vetter, J. Deming, P. Jumars, and B. Krieger-Brockett. A predictive model of bacterial foraging by means of freely released extracellular enzymes. *Microbial Ecology*, 36:75–92, 1998.

[35] G.H. Weiss. Overview of theoretical models for reaction rates. *Journal of Statistical Physics*, 42(1):3–36, 1986.

[36] G. Wilemski and M. Fixman. General theory of diffusion-controlled reactions. *The Journal of Chemical Physics*, 58:4009, 1973.

[37] C. L. Y. Yeong and S. Torquato. Reconstructing random media. *Physical Review E*, 57:495–506, 1998.

[38] R.M. Ziff. Flux to a trap. *Journal of Statistical Physics*, 65(5):1217–1233, 1991.